

Master's Programme in Electronics and Nanotechnology

Implementing Zinc-Air Batteries in Single-Use Clinical Monitoring Patches

Ida Forssell

Master's thesis
2025

Copyright ©2025 Ida Forssell

Author	Ida Forssell	
Title of thesis	Implementing Zinc-Air Batteries in Single-Use Clinical Monitoring Patches	
Programme	Master's Programme in Electronics and Nanotechnology	
Major	Microelectronic Circuit Design	
Thesis supervisor	Prof. Kari Halonen	
Thesis advisor(s)	Robert Santala, M.Sc. (Tech.)	
Collaborative partner	GE HealthCare Finland Oy	
Date	Number of pages	Language
26.05.2025	70 + 6	English

Abstract

In recent years, the interest in single-use electronics, particularly in the medical field, has increased due to their convenience and hygienic benefits. This thesis investigates the use of zinc-air batteries to power a single-use clinical monitoring patch. These batteries offer advantages such as environmental safety, affordability, compact size, long shelf life, and stable discharge voltage. However, challenges remain in monitoring battery depletion despite a stable voltage, optimising shelf life and operating conditions, and ensuring electrical isolation before activation.

To evaluate the effects of different operational conditions, zinc-air batteries were discharged using various current profiles. Shelf life was studied by storing batteries under different conditions and analysing their degradation through x-ray computed tomography and discharge testing. Several lifetime estimation methods were explored, including coulomb counting and response time analysis via equivalent circuit simulations. The correlation between battery weight changes and lifetime was also investigated. Additionally, simulations were conducted to assess the feasibility of various on/off battery control circuits, focusing on functionality and leakage current performance.

The longest lifetimes for zinc-air batteries were observed under constant current discharge, though fluctuating current profiles also proved viable, with lifetime only depending on the specific profile. Coulomb counting may be used for lifetime estimation if adjusted for battery aging, while response-time-based methods showed strong potential. Battery weight also correlated with discharge behaviour and could aid in estimating remaining life at assembly. X-ray imaging and discharge testing revealed that properly sealed storage methods can preserve battery function for up to two years. Several transistor-based switching circuits were shown to effectively isolate the battery when idle, though real-world testing is needed for validation. Overall, this thesis demonstrates that zinc-air batteries are a feasible power source for single-use clinical monitoring patches, provided their characteristics are well understood and managed.

Keywords zinc-air battery, battery lifetime estimation, shelf-life optimisation, discharge current, equivalent circuit simulation, battery control circuit

Författare Ida Forssell

Titel Implementering av zink-luftbatterier i engångssensorer avsedda för medicinsk övervakning

Utbildningsprogram Magisterprogrammet i elektronik och nanoteknologi

Huvudämne Mikroelektronikdesign

Ansvarslärare Prof. Kari Halonen

Handledare Robert Santala M.Sc. (Tech)

Medarbetare GE HealthCare Finland Oy

Datum 26.05.2025

Sidantal 70 + 6

Språk Engelska

Sammandrag

Under de senaste åren har intresset för engångselektronik ökat särskilt inom den medicinska industrin tack vare deras praktiska och hygieniska fördelar. Detta diplomarbete undersöker användningen av zink-luftbatterier i engångssensorer avsedda för medicinsk övervakning. Dessa batterier erbjuder fördelar så som miljövänlighet, förmånlighet, liten storlek, goda lagringsegenskaper och stabil utgångsspänning. Däremot finns det utmaningar gällande övervakning av batteriets urladdning med en stabil utgångsspänning, optimering av lagringstid och operativa förhållanden samt elektrisk isolering av batteriet före sensorn aktiveras.

För att utvärdera olika operativa förhållanden urladdades zink-luftbatterier med varierande strömprofiler. Batteriernas lagringstid undersöktes genom att förvara dem i olika förhållanden och sedan analysera dem med röntgenbaserad datortomografi och urladdningstest. Flera metoder, inklusive coulomb-räkning och responstidsanalys via en ekvivalent kretsmodell, utforskades för att uppskatta batteriernas livslängd. Sambandet mellan batteriets viktförändring och livslängd undersöktes också. Dessutom genomfördes simuleringar, med ett fokus på funktionalitet och läckageström, för att bedöma lämpligheten av olika batterikontrollkretsar.

De längsta livstiderna för zink-luftbatterier uppnåddes då batterierna urladdades med konstant ström. Även varierande strömprofiler visade sig fungera, men då berodde livslängden på den specifika profilen. Coulomb-räkning är användbart om batteriets åldrande beaktas och responstidsmetoden visade stort potential. Batteriernas vikt visade ett samband med urladdningsbeteende och kan bidra till att uppskatta återstående livslängd vid montering. Röntgenbilder och urladdningstest visade att lagringsmetoder som effektivt skyddar mot omgivande luft kan bevara batteriets funktion i upp till två år. Flera transistorbaserade batterikontrollkretsar visade god förmåga i att isolera batteriet i viloläge, även om test i verkliga förhållanden krävs för att bekräfta resultaten. Detta diplomarbete visar övergripande att zink-luftbatterier är en lämplig strömkälla för engångssensorer avsedda för medicinsk övervakning, förutsatt att deras egenskaper förstås och hanteras korrekt.

Nyckelord zink-luftbatteri, batterilivslängdsuppskattning, optimering av lagringstid, urladdningsström, simulation av ekvivalent krets, batterikontrollkrets

Table of contents

Preface and acknowledgements	7
Symbols and abbreviations.....	8
Symbols	8
Abbreviations	8
1 Introduction	9
2 Literature review	11
2.1 Implementation and application context	11
2.2 Battery structure	13
2.3 Discharge dynamics and lifetime estimation	15
2.3.1 Discharge process and reactions	15
2.3.2 Understanding the discharge curve	16
2.3.3 Environmental factors affecting discharge	18
2.3.4 Methods of estimating battery lifetime	20
2.4 Electrical behaviour of zinc-air batteries.....	24
2.4.1 Operational characteristics and limitations.....	24
2.4.2 Equivalent circuit model	26
2.4.3 On/off battery control circuit	29
3 Methodology.....	36
3.1 Discharge measurements with constant current.....	36
3.2 Discharge measurements with fluctuating current.....	37
3.3 Shelf-life aging of batteries	38
3.4 Equivalent circuit modelling and response time analysis.....	39
3.5 Battery weight measurements	39
3.6 Investigation of battery aging through x-ray computed tomography	40
3.7 Simulation of on/off battery control circuits.....	41
4 Results and discussion	42
4.1 Impact of discharge conditions and aging on battery lifespan	42
4.1.1 Discharge with constant current.....	42
4.1.2 Discharge with fluctuating current	43
4.1.3 Discharge of aged batteries	48

4.2	Methods of estimating state of charge.....	52
4.2.1	Coulomb counting	52
4.2.2	Equivalent circuit modelling and response time analysis	54
4.2.3	Battery weight.....	58
4.2.4	Investigation of battery aging through x-ray computed tomography	60
4.3	Simulation of on/off battery control circuits.....	64
5	Conclusions and recommendations for future work	71
	References.....	73
A.	LabVIEW program for producing fluctuating discharge currents	79
B.	Storage methods for shelf-life battery aging.....	80
C.	Equivalent circuit modelling results	83
D.	Cross-sectional CT images of zinc-air batteries.....	84

Preface and acknowledgements

This thesis was carried out between September 2024 and May 2025 at GE HealthCare. I would like to thank everyone who supported me during this time. I'm especially grateful to my advisor, Robert Santala, for his guidance and for offering me the opportunity to work on this interesting topic. His feedback and suggestions were invaluable. I also want to thank my supervisor, Professor Kari Halonen, for his support throughout the process. His practical advice and genuine interest in the topic were both encouraging and helpful during the work.

A special thanks goes to Ville Vartiovaara for his technical expertise and for always being willing to help when I had questions or needed input. His input made a big difference. Thanks also to my colleagues at GE HealthCare for creating a helpful and encouraging work environment. I appreciated all the help and support.

Finally, I want to thank my friends and family for their patience, encouragement, and kind words during this project. It meant a lot.

Helsinki, May 19th 2025

Ida Forssell

Symbols and abbreviations

Symbols

C	Capacitance
I	Current
R	Resistance
t	Time
U	Voltage
V	Voltage
Vol	Volume
ρ	Density
τ	Time constant/response time

Abbreviations

BJT	Bipolar junction transistor
CPP	Cast polypropylene
CT	Computed tomography
EIS	Electrochemical impedance spectroscopy
ESD	Electrostatic discharge
GPIO	General purpose input output
IC	Integrated circuit
MCU	Microcontroller unit
MOSFET	Metal-oxide-semiconductor field-effect transistor
OPP	Oriented polypropylene
PMU	Power management unit
SMU	Source measure unit
SoC	State of charge
UVLO	Undervoltage-lockout

1 Introduction

In recent years, the interest in single-use electronics, particularly in the medical field, has increased due to their convenience and hygienic benefits. Disposable sensors, which are used and then discarded, are especially beneficial in clinical settings as they help limit the spread of infection between patients [1]. However, powering these single-use devices wirelessly present unique challenges, especially in terms of environmental impact, cost-effectiveness, and performance. This thesis explores the option of using zinc-air batteries to power single-use clinical monitoring patches.

Zinc-air batteries are an attractive option for this application due to their environmental safety, affordability, compact size, long shelf life, and stable discharge voltage [2, 3]. Additionally, zinc is abundant and inexpensive, further increasing the appeal of zinc-air batteries for single-use electronics [4, 5].

Despite the many advantages, zinc-air batteries present several challenges that must be addressed to optimize their use in single-use sensors. One major challenge is accurately monitoring the battery state of charge [6]. Zinc-air batteries maintain a relatively constant discharge voltage, making traditional voltage-based depletion indicators inaccurate [5]. Another challenge is optimising both storage and operational conditions to ensure the battery retains its charge until it is needed and maximises its lifespan. Furthermore, various strategies must be implemented in the device to manage the battery, address potential electrical behaviour challenges, optimise performance, and ensure safety.

This thesis aims to address these challenges by investigating the various aspects of implementing zinc-air batteries in single-use clinical monitoring patches. The research objectives include establishing a method to monitor battery depletion with a flat discharge curve, optimising shelf life through improved storage conditions, and considering the impact of various operational conditions. Additionally, this thesis explores a circuit solution to isolate the battery before the device is activated and facilitate its connection when the device is ready for use.

This thesis examines the effects of different variables on battery lifetime by measuring the discharge curve under various conditions, such as the surrounding environment and varying load conditions. Other measurements, including X-ray analysis and weight assessment, will be used alongside the discharge curve measurements to investigate these effects. The accuracy and applicability of various lifetime monitoring methods is also evaluated in relation to the discharge curve measurements. Finally, the functionality of the circuit solution is evaluated.

The remainder of this thesis is divided into 4 chapters. Chapter 2 reviews the literature on the concepts and background theory utilized while Chapter 3 describes the used methodology. Chapter 4 explains the experimental

results of the thesis, including discharge curves and the circuit implementation. Chapter 5 concludes the present thesis by discussing the optimal implementation methods of a zinc-air battery and by recommending future work.

2 Literature review

2.1 Implementation and application context

Primary zinc-air batteries are commonly used in medical equipment where small size is essential, current consumption is very low, and the device operates continuously until the battery is depleted. Typical healthcare applications include hearing aids and medical telemetry transmitters [7, 8]. This thesis examines the use of zinc-air batteries in single-use wireless clinical monitoring patches, which continuously measure patient data until the battery is depleted. The patch is then disposed of.

One notable example of a comparable healthcare device to the one discussed in this thesis is the Abbott FreeStyle Libre continuous glucose monitoring system. This single-use sensor is applied to the back of the upper arm and can be used continuously for up to 14 days. It measures glucose levels every minute using an amperometric electrochemical sensor and communicates the data to a smartphone via Bluetooth. Although powered by a silver oxide battery rather than a zinc-air battery, the general concept of the sensor is similar to the monitoring patch examined in this thesis [9, 10]. Figure 1 illustrates the Abbott FreeStyle Libre.



Figure 1: The Abbott FreeStyle Libre continuous glucose monitoring sensor [11]

Another example of a disposable wearable sensor is the Zio Patch. This long-term, wireless cardiac monitoring system records the electrical activity of the heart for up to 14 days. It is specifically designed to record cardiac arrhythmias. The device features a button that patients can press when experiencing symptoms of arrhythmia. Powered by two lithium manganese dioxide coin cells, the device has a shelf-life of six months [12, 13]. The Zio Patch is shown in Figure 2.

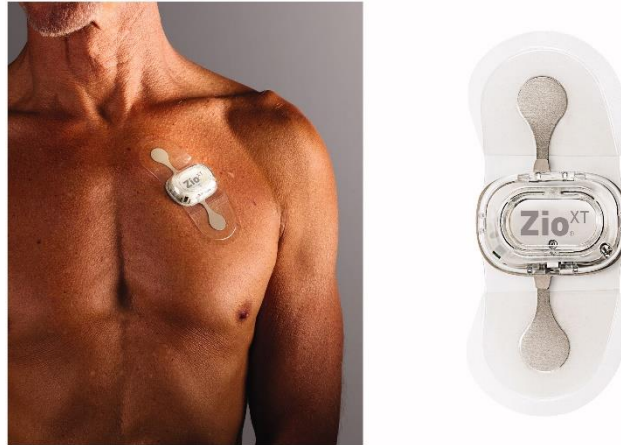


Figure 2: The Zio Patch wearable sensor [12]

This thesis explores the implementation of zinc-air batteries to power a device similar to the Abbott FreeStyle Libre and the Zio Patch. The single-use clinical monitoring patch is designed to continuously monitor a health parameter for approximately three days until the battery is depleted. It is intended for hospital use, where it will be used on a single patient and then disposed of, minimising cross-contamination between patients [1]. The patch communicates patient data to a host system via Bluetooth. It is wearable, wireless, and non-invasive. Given that hospitals are likely to purchase supplies in bulk, the device is also designed to have a long shelf-life to accommodate extended storage periods.

The clinical monitoring patch consists of three main components: the powering side, the sensor interface, and the wireless communication module. The sensor interface is responsible for collecting patient data. The wireless communication module contains the microcontroller unit (MCU) and transmits the data to a host system. The powering side supplies power to the entire circuit from the power source. This is primarily managed by the power management unit (PMU), which converts the input power into various signals to power the rest of the device. The PMU is equipped with communication capabilities connected to the sensor interface and the communication module to shut off in case of an error or fault in the device. Additionally, the PMU features a fuel gauge, which includes a coulomb counter and measures battery voltage, individual supply voltages, and junction temperature.

The general function of the patch is illustrated by a block diagram in Figure 3. The sensor is powered by three zinc-air batteries connected in series, providing a total voltage of approximately 3.75V as shown in Chapter 4.1.1. This voltage serves as the power input for the PMU, which routes it to the power converters and the fuel gauge for monitoring. The battery voltage and current are measured, and the coulomb counter tracks discharged capacity by integrating current consumption over time. The fuel gauge also monitors the voltage of an individual battery cell to detect if one is discharging faster

than the others. The device's overall power consumption is approximately 3mA. However, the communication and sensor interface blocks operate at certain frequencies, causing current fluctuations during operation. The device will function as long as the battery voltage remains above the programmed under-voltage lockout (UVLO) threshold of approximately 1.8V.

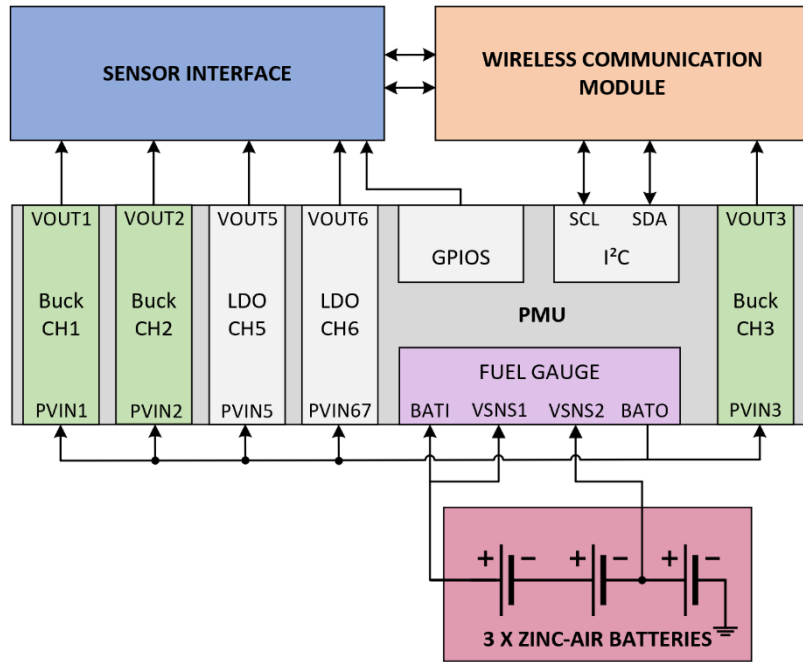


Figure 3: Block diagram of the single-use clinical monitoring patch

2.2 Battery structure

Zinc-air batteries are a type of metal-air battery that utilizes zinc as the anode and oxygen from the surrounding air as the cathode [7]. One of the key advantages of zinc-air batteries is their high energy density. Because they only contain the anode within the cell, they can achieve twice the capacity of non-metal-air batteries of the same size [3, 14].

A zinc-air battery consists of three primary components: the anode, a separator, and the cathode, as illustrated in Figure 4 [15, 16]. These components are immersed in an aqueous alkaline electrolyte [8, 15]. The battery casing, which houses the components, is designed to be open at the cathode end to allow atmospheric oxygen to enter. This exposure to oxygen is essential for the functionality of the battery [2, 7]. The openings in the casing are initially sealed with a tab to prevent air from entering the battery until it is ready for use. Upon removal of the tab, the battery is exposed to the surrounding air, initiating the internal electrochemical reactions that cannot be reversed by reattaching the tab [7].

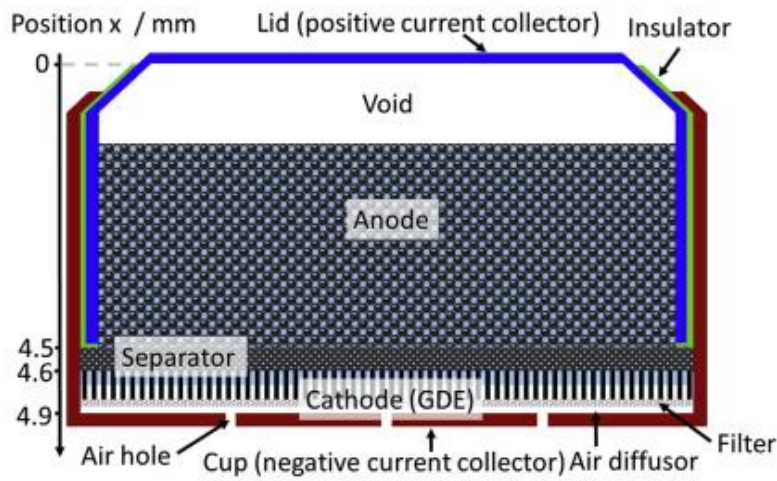


Figure 4: Structure of a zinc-air battery cell [17]

The anode consists of metallic zinc powder, which is immersed in an aqueous electrolyte. The zinc powder has a large surface area, promoting rapid and uniform dissolution of zinc during discharge [8, 17]. Generally, the battery performance is directly related to the surface area of the zinc granules, with a larger surface area reducing the internal resistance. However, increasing the surface area also makes the anode more susceptible to corrosion. Historically, alloying zinc with mercury was used to mitigate corrosion, but this practice has been largely abandoned due to environmental concerns [8, 18]. The volume of the zinc anode increases during discharge and the void space under the battery cover exists to accommodate this change [17].

The electrolyte, typically an aqueous potassium hydroxide solution, is crucial for battery performance [16, 17, 18]. It enhances ionic conductivity and promotes fast oxygen reduction kinetics, which are essential for the electrochemical reactions of the battery. While the composition of the electrolyte can vary between manufacturers, a 30%wt concentration is commonly used to achieve maximum ionic conductivity [8, 18].

The separator is a microporous membrane that prevents direct contact between the anode and the cathode, while allowing the electrolyte to pass through [8, 16]. Its low electrical conductivity ensures that the electrochemical reactions can occur without short-circuiting the battery. Meanwhile, its high ionic conductivity facilitates the transport of ions from the air electrode to the zinc electrode [8, 18].

The cathode supplies the cell with atmospheric oxygen while retaining the electrolyte within the battery [17]. This electrode can be divided into three layers: the gas diffusion layer, the catalytic active layer and the conductive current collector situated between these layers [16, 18]. The gas diffusion layer is exposed to the outside through small openings in the battery casing. Its porous but hydrophobic structure prevents liquid electrolyte from passing through, while facilitating oxygen diffusion through the pores. The catalytic

layer is hydrophilic and contains a catalyst, such as manganese oxide, to help reduce the dissolved oxygen [8, 16, 17, 18]. This layer is facing the inside of the battery and is immersed in electrolyte to allow transport of ions from the reaction sites [16]. The current collector is a metal grid that facilitates and connects the flow of electrons [18].

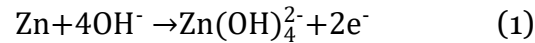
Overall, zinc-air batteries are composed of environmentally benign and low-cost components, making them an attractive option for single-use electronics [17, 19]. Their unique structure and composition enable them to deliver high energy density and stable performance, while their environmental impact remains minimal [8, 15, 17].

2.3 Discharge dynamics and lifetime estimation

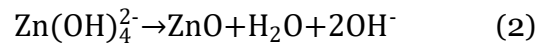
2.3.1 Discharge process and reactions

The discharge process of a zinc-air battery involves distinct reactions at the positive and negative electrodes. Together they form an electrochemical reduction-oxidation reaction, with the oxidation taking place at the anode and the reduction at the cathode. Understanding these reactions is crucial for optimising battery performance and longevity [20].

At the negative anode, zinc undergoes a series of reactions during discharge. Initially, solid zinc is oxidized into zincate ions that dissolve into the electrolyte [8, 15, 16]. This reaction is described in Equation 1 [8].



Once the zincate has supersaturated the electrolyte, the zincate ions begin to decompose, forming zinc oxide, water and hydroxide ions [4, 5, 8, 16]. This reaction is described in Equation 2 [8].



As zinc oxide precipitates it creates a porous layer on the zinc surface. This layer slows down the hydroxide supply and once all zinc is covered it causes a decline in cell voltage. Once the layer is too thick for hydroxide to get through it the electrode is completely passivated [16, 17].

At the positive air electrode atmospheric oxygen is dissolved into the electrolyte [15]. The dissolved oxygen is then reduced at the cathode catalytic sites [8]. It reacts with water and electrons from the zinc electrode, producing hydroxide ions [4, 5]. This reaction is described in Equation 3 [8].





The overall discharge reaction of the zinc-air battery can be summarized as shown in Equation 4 [8]. The entire discharge process is also described in Figure 5. The complete reaction theoretically yields a voltage of 1.65V. However, due to the internal resistance of the battery, the practical voltage is closer to 1.3V. The relatively constant internal resistance results in a largely flat discharge profile for the zinc-air battery [8, 16].

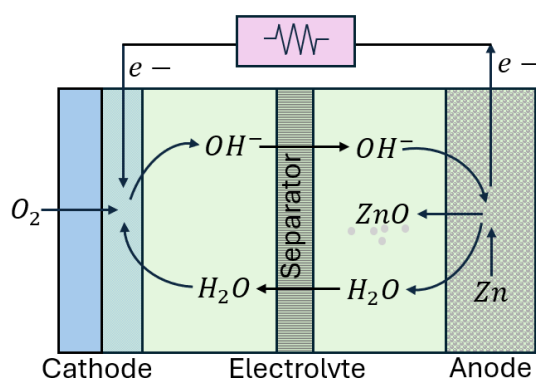


Figure 5: The complete reactions of a zinc-air battery during operation

2.3.2 Understanding the discharge curve

The overall discharge process of a battery can be described by a curve that represents the relationship between the battery's capacity or discharge time and its voltage output during the process. This discharge profile is a crucial indicator of the battery's performance and operational life [16]. For zinc-air batteries the discharge curve is notably flat, distinguishing them from non-metal-air batteries. The flat discharge curve indicates a stable internal resistance, which leads to a consistent battery voltage for most of its lifespan [6, 17]. The discharge curve of a zinc-air battery can be divided into four regions: initial voltage dip, voltage plateau, voltage step and voltage decay [16, 17]. An example of a zinc-air battery discharge curve displaying these regions can be seen in Figure 6.

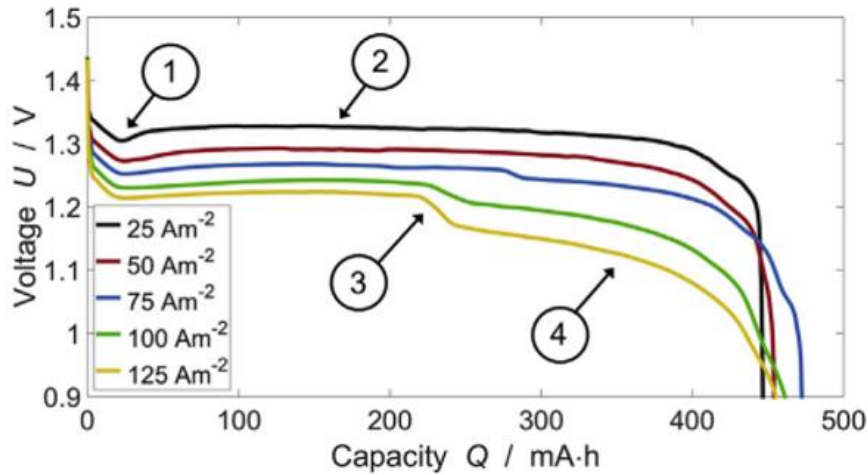


Figure 6: The discharge of a zinc-air battery measured at various current densities showing 1) The initial voltage dip, 2) The plateau phase, 3) The voltage step and 4) The voltage drop [17].

The initial voltage dip refers to a potential variation that occurs at the beginning of the discharge process at the same discharged capacity, regardless of the current [17, 16]. This voltage drop is caused when zincate ion formation consumes hydroxide ions without producing new ones, leading to an overpotential at the anode. Zinc oxide formation starts only after the electrolyte is supersaturated with zincate ions [8, 17, 18]. In addition, it can take up to a minute for enough air to reach the electrolyte before achieving a steady state for the oxygen reduction reaction. Once the reactions reach equilibrium the hydroxide ion production catches up to the rate of consumption and the discharge voltage recovers [5, 7, 17].

As the battery continues to discharge, the cell voltage stabilises, and the discharge process reaches a plateau [17]. The discharge voltage remains constant for most of the battery's operational life, and this duration is extended at lower discharge currents. This stability is due to the consistent internal resistance and the efficient electrochemical reactions within the battery [16].

Towards the end of the discharge curve, occasional voltage step-downs are visible. These voltage steps are more significant at higher discharge currents and barely visible at lower currents [17, 16]. The occurrence of these steps can be explained by the inhomogeneous nucleation of zinc oxide. During the voltage plateau, the battery consumes zinc that requires the least activation energy, such as exposed zinc closest to the separator. When a voltage step occurs, the easily accessible, low activation energy zinc is depleted. The battery then uses zinc with a higher activation energy, such as zinc covered in zinc oxide or located further away from the separator. Each time the battery switches to using zinc with a higher activation energy, it is visible as a step in the discharge curve [17, 21].

As the battery approaches the end of its life, the voltage drops rapidly. At this point, the battery is either running out of zinc or the activation energy for the remaining zinc is too high. The electrochemical reactions inside the battery suddenly become unable to sustain the necessary power output, causing the voltage to drop. The battery is considered depleted when the cell voltage drops below the cut-off voltage [17, 22].

The characteristics and performance of a zinc-air battery can largely be evaluated based on its discharge curve. A higher voltage and longer discharge time at a constant discharge current indicate better battery performance [21]. An ideal battery will reach the cut-off voltage very close to its theoretical capacity limit. However, in reality, the end of discharge is strongly influenced by degradation. In addition, higher discharge currents effectively decrease battery capacity because the consumption of zinc is limited to zinc with sufficiently low activation energy to sustain high output power. At lower currents, the discharge time is typically only limited by the amount of zinc in the battery [16, 17]. The initial voltage dip and the subsequent phases can exhibit slight variations based in changes in discharge conditions or battery properties [17]. However, the overall behaviour remains consistent, with a rapid voltage drop signalling the end of the battery's life [7].

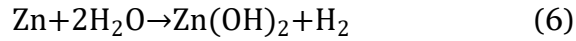
2.3.3 Environmental factors affecting discharge

Zinc-air batteries, while advantageous in many respects, are particularly sensitive to various environmental factors [2, 16, 23]. As long as the batteries are kept sealed in their original packaging, they have a long and stable storage life [7, 17]. A sealed battery loses approximately 2% of its capacity after one year in storage. However, once the battery is removed from its packaging and exposed to ambient air, several factors can negatively impact its operation. Understanding these factors is crucial for optimizing the battery's functionality and longevity [2, 7, 23].

One of the primary environmental factors affecting the lifetime of zinc-air batteries is the presence of carbon dioxide [2, 8, 18]. Carbon dioxide can dissolve in the electrolyte, leading to the formation of carbonates [16, 17, 21]. The carbonate reaction reduces hydroxide concentration, thus neutralizing the electrolyte and reducing its conductivity [16, 17, 23]. This decreases the solubility of both zincate and oxygen, inhibiting further discharge reactions. Carbonates can also precipitate as solid crystals, that can block pores in the air electrode and hinder its activity. All these factors significantly impact battery lifetime. The carbonate formation reaction is described in Equation 5 [8, 16, 17, 18].



The humidity levels in the ambient air can significantly impact the properties of the electrolyte [8, 23]. Zinc-air batteries have a good tolerance for humidity, with an optimal level of around 60% relative humidity. In humidity above the optimal level, excess water can flood the electrolyte [3, 8, 23, 24]. Increasing the water content in the electrolyte lowers its concentration, resulting in reduced ionic conductivity and, consequently, performance degradation [8, 16]. The increased water content also raises the likelihood of zinc reacting with water molecules, producing zinc hydroxide and hydrogen gas [17, 18]. This hydrogen evolution reaction is described in Equation 6. The reaction with water also decreases the capacity of the battery by consuming zinc [8, 21].



Below the optimal humidity level, the battery's lifetime is limited by water loss, which can lead to the electrolyte drying out [23, 24]. As water evaporates, the electrolyte concentration increases, making the battery more prone to corrosion and eventually causing it to cease operating [2, 16].

Temperature significantly influences the discharge reactions of zinc-air batteries. Operating these batteries at higher ambient temperatures can enhance their performance to a certain extent [3, 16]. Higher temperatures also increase the solubility of carbonates, mitigating the harmful effects of carbonate precipitation. However, elevated temperatures also lead to increased water loss and self-corrosion [8]. This is particularly relevant during the manufacturing process, where components are often exposed to high temperatures. Triggering harmful internal reactions during assembly can reduce the battery's overall capacity and effectiveness [2, 16].

Long storage times lead to shortened discharge time and reduced voltage levels. Over extended periods, the battery has more opportunities to interact with ambient air in harmful ways [2, 16, 23]. Additionally, prolonged exposure of zinc to the electrolyte can cause spontaneous corrosion through the hydrogen evolution reaction described in Equation 6. Given sufficient time, the battery can also self-discharge, if it is exposed to enough oxygen [2, 8, 16].

Controlling humidity and temperature during storage and use can help maintain the battery's integrity and prolong its lifespan [16, 23]. Due to the battery's semi-open structure, some harmful interaction with the environment is inevitable [2, 8]. Using batteries with smaller or fewer holes can limit ambient air access during storage and use, but this may restrict air intake [2, 14]. However, since the battery only needs oxygen during discharge, it can be isolated from ambient air when not in use to mitigate water vapor transpiration and carbon dioxide pickup. Limiting the battery's access to air when in

storage will also reduce its self-discharge. While it is more challenging to control the ambient environment during operation, reducing carbon dioxide and increasing oxygen levels can extend the battery's lifespan [2, 23].

2.3.4 Methods of estimating battery lifetime

The state of charge of the battery indicates the available capacity as a percentage of its nominal capacity [4, 25]. Accurately measuring the state of charge is important for knowing how much power remains in a device and preventing it from unexpectedly shutting down due to low power [25, 26]. There are various methods for estimating or measuring the state of charge, but their effectiveness, including how well they work, their suitability, and their accuracy, depends greatly on the specific battery type and the requirements of the device in which they are used [26, 27].

Direct measurement methods for measuring the state of charge are the most commonly implemented. These methods are simple, low-power, and inexpensive because they determine the state of charge directly based on a parameter with a known relationship with the battery's charge level. Using parameters such as open circuit voltage and impedance is common as they often exhibit a near-linear relationship with the state of charge [4, 20, 26]. However, zinc-air batteries have a very steady internal resistance, so none of the related parameters show any meaningful relationship with the rate of depletion [6, 7].

Measuring the step response of the battery voltage can be considered a direct measurement method [4, 20]. By subjecting a battery to a stepwise discharge current, the battery voltage will exhibit a delayed response before stabilising at a new level. This delay, known as the step response, increases exponentially as the battery is depleted. This relationship between the step response and the battery's state of charge also applies to zinc-air batteries. Figure 7 shows the relationship between the step response and the state of charge. Figure 7 also demonstrates that the step response can be measured from both the rising and falling edges, although they exhibit slightly different relationships with the state of charge [20, 27].

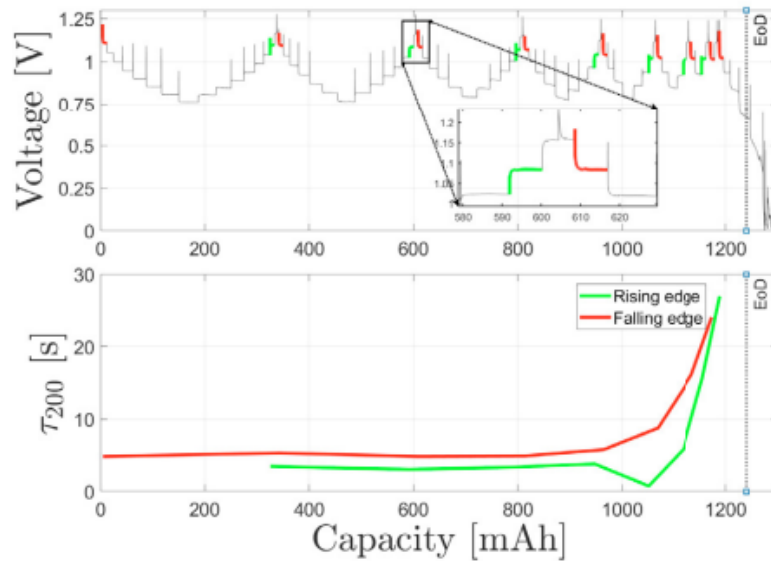


Figure 7: The estimated voltage profile and time constant values calculated for a 200mA current setpoint in function of the capacity of a zinc-air battery [27]

Electrochemical impedance spectroscopy (EIS) is another direct measurement method. This method involves subjecting the battery to a discharge current with varying frequencies and measuring its impedance throughout the frequency range [4, 26, 28]. The impedance of a zinc-air battery cell depends on the frequency and changes as the battery depletes [4, 20]. The state of charge of a battery can therefore be inferred by measuring its impedance at a specific discharge current frequency and comparing it with the electrochemical impedance spectroscopy profiles of batteries at different states of charge [26]. The result of an EIS measurement is a Nyquist plot that displays the battery impedance across a frequency range, as shown in Figure 8. This method is usually more expensive compared with estimating the state of charge by measuring the step response [4, 28].

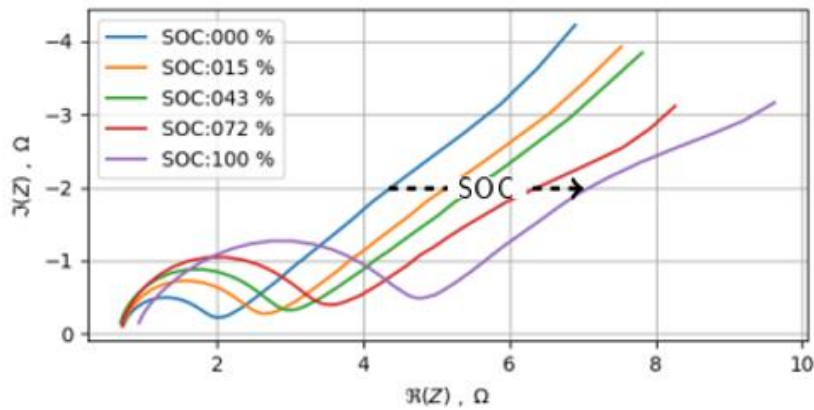


Figure 8: Nyquist plot of primary zinc-air batteries (type PR13) at 21°C, obtained with an AC amplitude of 5mA and an overlaid DC current of 5mA, across a frequency range of 0.1Hz to 1MHz [28]

Coulomb counting is known as a bookkeeping method for estimating the battery's charge [4, 26]. This method monitors the discharged current and elapsed time to determine the remaining capacity, effectively counting the number of Coulombs consumed. In practice, this is achieved by integrating the discharge current over time. Coulomb counting can be highly accurate and very easy to implement, but it requires precise knowledge of the battery's total capacity, the exact current profile, and the initial capacity, which can vary in primary zinc-air battery cells [25, 26]. Coulomb counters also cannot account for self-discharge or other parasitic internal reactions within a battery that might reduce its capacity [20].

State of charge estimation is typically accomplished using specific battery models. This process can involve deriving a parameter within the battery model from active measurements taken while the battery is being depleted [4, 25, 27]. The parameter value can then be used to estimate the state of charge based on the known behaviour of the battery [25, 27]. Alternatively, multiple parameters can be combined for increased accuracy [26]. Electrochemical battery models, for example, can accurately describe both kinetic and charge transfers within a battery to estimate the state of charge. However, they use numerous parameters and differential equations, which require significant computational power [25].

An equivalent circuit model can also be employed to describe the behaviour of a battery and determine its state of charge. This model simplifies the complex electrochemical processes into an electrical circuit comprised of resistors, capacitors and other components [4, 25, 28]. The equivalent circuit parameters change with different operational conditions, such as state of charge or temperature. There are also more complex models involving machine learning or AI, which are particularly useful in high power applications where state of charge accuracy is crucial. These advanced models can analyse

vast amounts of data to predict the state of charge with high precision, but they require substantial computational resources [25].

The state of charge of a zinc-air battery can also be measured through physical and chemical changes in its structure. While these methods are not practical for real-world applications, they can be useful for determining the state of charge in an experimental setting. As the battery depletes, changes in the electrolyte concentration and reaction rates provide a reliable method for determining the battery's rate of depletion in a laboratory environment [27]. Additionally, during discharge the denser zinc transforms into the less dense zinc oxide. These two substances can be distinguished as materials with different densities in an x-ray, allowing the state of charge to be determined based on the extent of zinc's transformation into zinc oxide. Figure 9 illustrates an example of determining the state of charge in zinc-air battery cells using x-ray computed tomography. However, this method of determining the state of charge is only accurate at low discharge currents. At higher discharge currents, not all the zinc is utilised, leading to incomplete depletion and inaccurate results [5, 15].

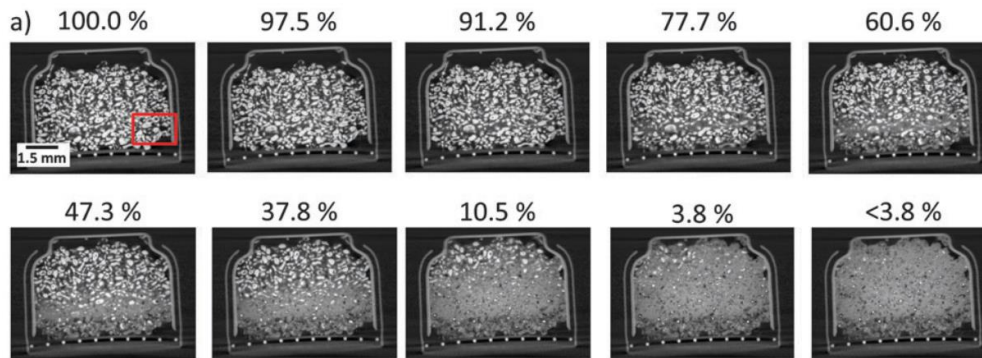


Figure 9: State of charge determination of zinc-air battery cells using x-ray computed tomography [5]

As the battery depletes, the increasing amount of the less dense zinc oxide causes the volume inside the battery to increase linearly. The state of charge can be represented as a function of the zinc volume, as can be seen in Equation 7. When the battery is fully depleted, its volume increases by up to 27% compared to when it is at full capacity. This change can also be seen in an x-ray. Additionally, as the battery binds oxygen during discharge, its mass increases linearly. Therefore, the battery's capacity can be determined by its change in mass, provided there is no input or output of other substances like carbon dioxide or water that could alter the mass [5, 15].

$$\text{Vol}_{\text{disch}} = \frac{It}{\rho C} + \text{Vol}_{\text{initial}} \therefore \text{Vol}_{\text{disch}} \propto t \quad (7)$$

where

$\text{Vol}_{\text{disch}}$ = volume of zinc after the battery is discharged (mm^3)

I =discharge current (mA)

t =time (h)

ρ =density of zinc (g/mm³)

C =theoretical capacity of zinc (mAh/g)

$Vol_{initial}$ =initial volume of zinc in the battery (mm³)

2.4 Electrical behaviour of zinc-air batteries

2.4.1 Operational characteristics and limitations

In the development of battery-powered devices, the primary consideration is optimising the lifetime of the battery. This is crucial because it determines the effective utilisation time of the device. The system's lifetime is partly dictated by the battery capacity [22, 29, 30]. Battery capacity can be represented in three ways: the theoretical capacity, the standard capacity, and the actual capacity. The theoretical capacity is the maximum energy the battery could provide under ideal conditions. The standard capacity, typically listed in the battery's datasheet, represents the nominal capacity when the battery is discharged under load conditions specified by the manufacturer. The actual capacity is the energy a battery can deliver under a given load, and it is used to judge the efficiency of a system with that load [29, 31].

The battery lifetime and device's lifespan are also determined by the energy consumption of the system. This consumption refers to both the amount of energy and the specific load profile of the system [22, 29, 31]. Higher discharge currents result in lower battery voltage and shorter battery lifespan, not only by depleting the battery faster but also reducing usable capacity [15, 22]. Conversely, lower discharge currents lead to higher battery voltage and longer battery lifespan. Generally, if the current consumption occurs at the same nominal value, the battery lifetime will be consistent regardless of the specific current profile [22]. However, in practice, the battery's lifespan can vary by up to 25% even at the same mean current consumption [31].

The battery behaviour under different load conditions can be explained by two effects: the rate capacity effect and the recovery effect. The rate capacity effect describes how the amount of anode material consumed depends on the discharge current. At low currents, the anode material is consumed evenly until the battery runs out of material. However, at high currents, the battery can only consume the material closest to the cathode. This effect explains how higher discharge currents result in shorter battery lifetimes [22, 29, 31].

The recovery effect in the battery can be attributed to the generation and consumption of hydroxide ions. During discharge, the anode consumes hydroxide ions while the cathode produces them. This creates a concentration gradient between the electrodes, causing the ions to diffuse from the cathode to the anode to replace the consumed ions [29, 32]. At high discharge currents, the ions cannot diffuse quickly enough to replace the consumed ones, leading

to a potential difference between the poles that degrades the output voltage. However, if the battery is left idle between periods of high current, the diffusion can catch up, allowing the ion concentration to even out. This process increases the battery’s capacity and extends its lifetime [22, 29].

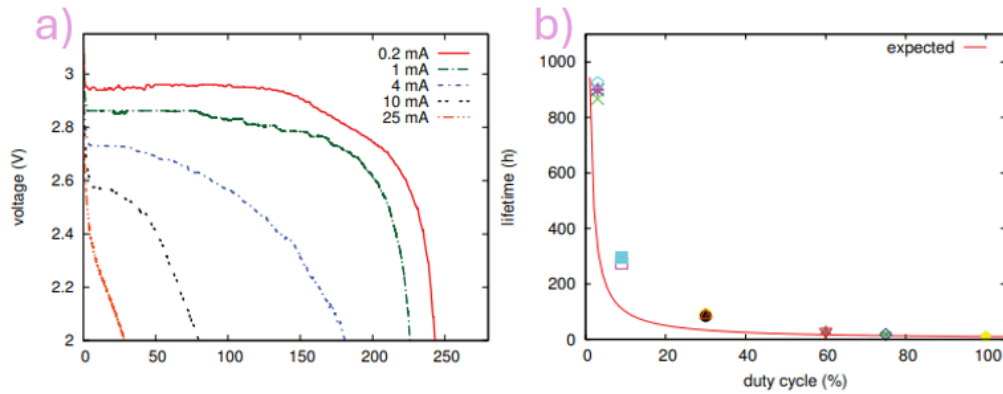


Figure 10: Demonstration of a) rate capacity effect and b) recovery effect in primary lithium-ion batteries [22]

The recovery effect and the rate capacity effect, both illustrated in Figure 10 for lithium-ion batteries, create a trade-off in battery lifetime when the load is non-uniform with a constant mean current. Longer idle times can extend the battery’s lifespan, but they also lead to higher current spikes that shorten it [22, 31]. To maximise lifespan, the system’s idle times and current spikes should be adjusted to make idle periods as long as possible while keeping current spikes low enough to minimise their negative effects [22, 29].

In addition to maximising the utilised capacity of the battery, the device’s lifespan can be extended by minimising power consumption. The goal is to extend the battery’s lifetime as much as possible while still meeting performance requirements [22, 29, 31]. This involves understanding and optimising the device’s load profile and minimising sources of power dissipation. Power dissipation is primarily caused by the charging and discharging of capacitances and leakage currents in transistors. In devices with long shelf lives, leakage currents can significantly reduce lifespan by consuming the battery. Therefore, it is crucial to minimise power consumption, especially during inactivity [29, 33].

Several other factors can affect the applicability and performance of zinc-air batteries in a device. These batteries do not tolerate high currents well, especially if the current is elevated for an extended period, necessitating protective measures such as a fuse to prevent damage from overcurrent conditions [8, 14]. Moreover, the battery voltage varies during discharge, but the need for mitigation depends on the device’s sensitivity to voltage fluctuations [17]. Implementing an under-voltage lockout can manage the final drop in voltage, preventing the device from exposure to undervoltage conditions [4].

Furthermore, UVLO helps prevent deep discharge of the battery, which occurs when more than 80% of the battery is depleted [30].

Lastly, zinc-air batteries exhibit the double layer effect, where a charge zone forms between the zinc electrode and the electrolyte due to positive zinc ions at the electrode surface and negative hydroxide ions in the electrolyte. This effect causes the battery to behave like a capacitor, effectively filtering high-frequency input signals and maintaining steady output voltage at sufficiently high frequencies [32].

When using zinc-air batteries as the power source in a device, it is important to understand their behaviour in a circuit. Many electrical behaviours associated with batteries, such as rate dependent capacity and charge recovery, can be generalised across different types, regardless of their exact chemistry. However, the specific electrical characteristics are unique to each type of battery. There is limited research quantifying these properties for inexpensive primary batteries, such as zinc-air batteries [22].

2.4.2 Equivalent circuit model

Equivalent circuit models of batteries aim to describe their electrical behaviour using circuit components, each representing a specific aspect of the battery's operation. Together, these components simulate realistic performance, providing a straightforward and cost-effective method to estimate the battery's characteristics [4, 28, 34]. This approach is essential for effective battery management in various applications [4, 25].

The behaviour of a zinc-air battery can be modelled using a Thevenin equivalent circuit. As shown in Figure 11, this circuit includes an ideal voltage source, a series resistance, and a parallel RC pair. The ideal voltage source (U_{OC}) represents the open circuit voltage of the battery, the series resistance (R_i) represents the internal resistance of the battery, and the parallel RC pair describes the non-linear polarisation response of the battery [4, 30, 34, 35]. The internal resistance arises from both the electrolyte and connection resistance [34]. The non-linear polarisation response refers to the dynamic behaviours caused by varying ion concentrations within the battery [30]. These varying ion concentrations induce effects such as the recovery effect and the double layer effect [29, 32]. Therefore, the capacitor represents the capacitive effect of the cell, while the parallel resistance represents the charge transfer resistance associated with that effect [30, 35]. In addition, U_{cell} denotes the terminal voltage, while I_{cell} represents the current flow through the attached load [4, 34].

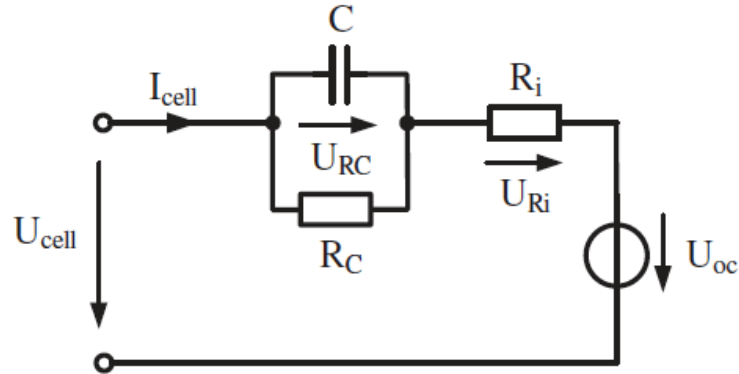


Figure 11: Equivalent circuit model of a zinc-air battery cell [4]

The values of the components in the equivalent circuit depend on various battery states, such as the state of charge. To determine these component values and assess the state of charge, several direct measurement methods can be employed. For instance, the open circuit voltage can be determined by measuring the steady-state voltage of the battery when no current is flowing [4, 20, 26]. Additionally, the series resistance can be measured by observing the voltage drop when the battery is connected to a load [35]. EIS is another method that can be used to determine the resistor values corresponding to different frequency components [4, 26]. The voltage step response of the battery, when subjected to a current pulse, can be used to determine the equivalent circuit component values [4, 20, 34].

EIS sweeps the battery discharge current through a range of frequencies to identify resistance components associated with specific frequency ranges. The simplest equivalent circuit includes a single parallel RC pair to account for the dynamic response [4, 26, 28, 34]. However, to create a more comprehensive model, the equivalent circuit can incorporate multiple RC pairs, each accounting for the dynamic response at different frequency ranges [28, 34]. Figure 12 describes the various resistances, each associated with its specific frequency range. The internal resistance (R_o) varies quadratically with the battery's state of charge. The first RC pair resistor (R_1) has a linear relationship with the state of charge and is believed to represent the increasing resistance as zinc oxidises to zinc oxide. The second RC pair resistor (R_2) is associated with the diffusion process within the battery [28].

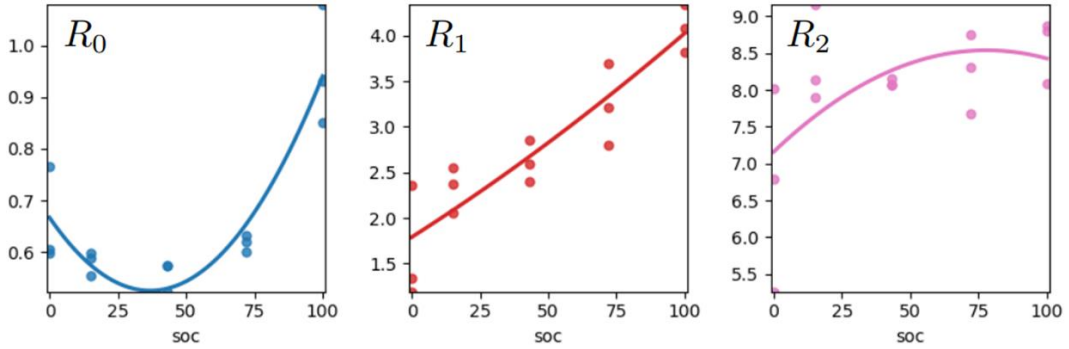


Figure 12: Equivalent circuit resistance components identified through EIS in relation to the state of charge [28]

The RC pair in the circuit determines the voltage step response of the battery. Figure 13 illustrates the relationship between the circuit components and the voltage step response. In the figure, the current is negative because it is being drawn from the battery rather than supplied to it. Therefore, at the peak (I_{pulse}), the current is closest to zero. The corresponding voltage recovery peak includes a voltage (ΔU_{Ri}), attributed to the series resistance. The remainder of the voltage peak (ΔU_C) is attributed to the charging or discharging of the capacitor (C). The initial slope of the capacitor charging phase is used to determine the time constant (τ), which describes how quickly the voltage responds to the current step. As the battery depletes, the resistance (R_C) increases, which in turn increases the time constant. Consequently, the voltage takes longer to reach its peak. The relationship between the capacitance, resistance and time constant is described in Equation 8. Both the time constant and the resistance (R_C) can be used to determine the state of charge [4, 34, 35].

$$\tau = R_C \cdot C \quad (8)$$

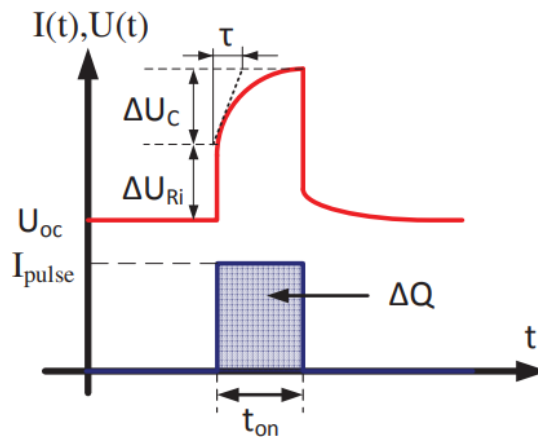


Figure 13: Relationship between the voltage step response and the equivalent circuit parameters [4]

Equivalent circuit models of batteries are typically integrated into battery management systems [4, 25]. Various battery characteristics are measured during operation. These measurements can be used to assign values to the equivalent circuit components, which have a known relationship with the battery's state of charge [20, 25]. This allows for real-time estimation of the state of charge in battery-powered devices [20, 26]. However, the equivalent circuit model does not account for long-term effects such as self-discharge or corrosion [34].

2.4.3 On/off battery control circuit

In battery-powered devices, it is crucial to ensure that the batteries are only connected to the rest of the circuit once the device is activated. Electrically isolating the batteries prevents them from draining while the device is idle, thereby extending the device's lifespan [36, 37]. Figure 14 shows a block diagram of the single-use clinical monitoring patch, which includes a block for a circuit designed to connect and disconnect the batteries. This patch requires a method for the user to activate and possibly deactivate it, achieved through a switch that controls the battery connection circuit. Moreover, the device uses a control signal from the MCU in the wireless communication block to provide final permission for the device to activate and for the circuit to keep the batteries connected. Other connections between the batteries and the rest of the circuit, such as the fuel gauge monitoring of an individual battery, need to be disconnected while the device is inactive to minimise leakage currents.

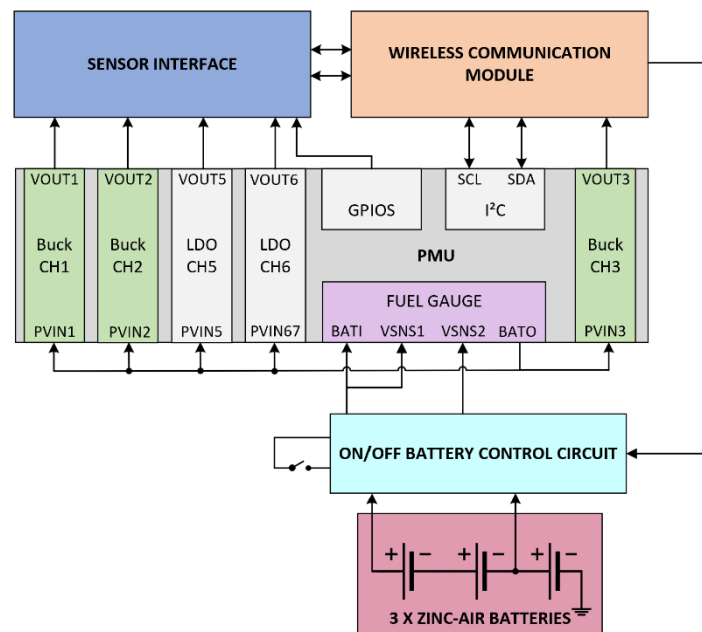


Figure 14: Block diagram of the clinical monitoring patch with an on/off battery control circuit

A mechanical switch can connect and disconnect components in a circuit, but it cannot be controlled by a control signal. Additionally, its contacts tend to bounce when it is activated, causing the circuit to rapidly connect and disconnect multiple times. Therefore, additional circuitry is required that uses a momentary switch solely for activation. A suitable solution is a transistor circuit, where a switch controls the conduction in a transistor positioned between the battery and the rest of the circuit. Once activated, the device maintains the transistor's conduction without relying on the switch. Several factors must be considered when designing the transistor circuit, including necessary functionalities and operational limitations [36].

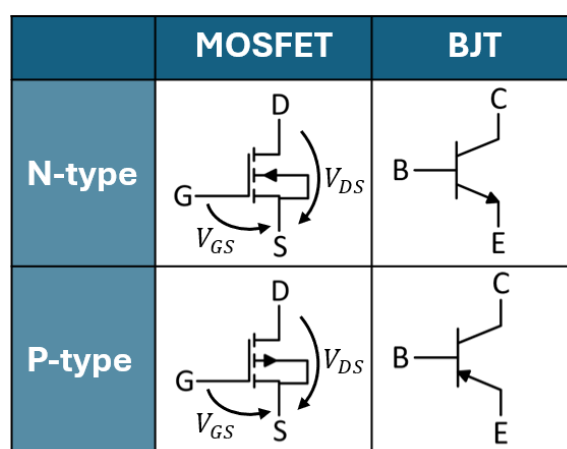


Figure 15: The symbols and equivalent terminals of n-type and p-type MOSFETs and BJTs, figure recreated based on [36]

Transistors are three-terminal semiconductor devices where one terminal controls the conduction between the other two. The two most common types are bipolar junction transistors (BJTs) and metal-oxide-semiconductor field-effect transistors (MOSFETs) [36, 37]. Although their specific structures and underlying principles of operation differ, their basic function remains the same. Both MOSFETs and BJTs can be either n-type or p-type, depending on whether their majority charge carrier is a negatively charged electron (n-type) or a positively charged electron vacancy (p-type) [37]. An n-type transistor conducts when the controlling terminal is positive relative to the reference terminal, while a p-type transistor conducts when the controlling terminal is negative relative to the reference terminal. Figure 15 illustrates the symbols for both n-type and p-type MOSFETs and BJTs, along with their equivalent terminals [36, 37].

NMOS regions of operation	
Cutoff Region	$V_{GS} < V_{th}$
Triode Region	$V_{GS} > V_{th}, V_{DS} < V_{GS} - V_{th}$
Saturation Region	$V_{GS} > V_{th}, V_{DS} \geq V_{GS} - V_{th}$

BJT npn modes of operation		
Mode	Emitter-base junction	Collector-base junction
Cutoff	Reverse biased	Reverse biased
Active	Forward biased	Reverse biased
Saturation	Forward biased	Forward biased

Figure 16: Conditions for the operating regions of n-type transistors, figure recreated based on [37]

Figure 16 describes how BJTs and MOSFETs operate in different regions. In MOSFETs, the voltage at the controlling terminal, called the gate, regulates conduction between the drain and the reference terminal, called the source [36, 37]. When a MOSFET functions as a switch, it transitions between the cutoff region and the triode region. For an n-type MOSFET (NMOS), the transistor does not conduct when the gate-to-source voltage (V_{GS}) is below the threshold voltage (V_{th}). To move the NMOS into the triode region, the gate-to-source voltage must exceed the threshold voltage. Additionally, the drain-to-source voltage (V_{DS}) must be lower than the difference between the gate-to-source voltage and the threshold voltage to avoid entering the saturation region. The threshold voltage value varies depending on the transistor [37].

In BJTs, the current at the controlling terminal, called the base, regulates conduction between the collector and the reference terminal, called the emitter [36, 37]. When a BJT functions as a switch, it transitions between the cutoff region and the saturation region. For an n-type BJT (nnp), the transistor is in the cutoff region when both the emitter-base junction and the collector-base junction are reverse biased. To move the npn into the saturation region, both junctions must be forward biased. A junction is reverse biased when the base voltage is lower than the other terminal, and forward biased when the base voltage is higher. The exact voltage difference required depends on the transistor, but typically the base needs to be at least 0.7V higher than the emitter for the transistor to conduct. Figure 16 lists all the criteria for keeping an n-type transistor in a specific operating region. By reversing these criteria, you can determine the conditions for a p-type transistor [37].

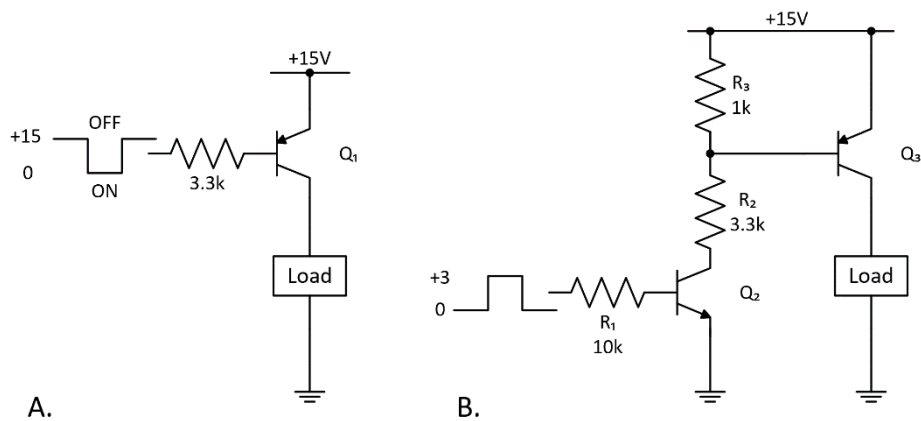


Figure 17: BJT circuits to switch the high side of a load returned to ground, figure recreated based on [36]

Figure 17 illustrates two transistor switch circuits where BJTs control the connection between a load and power supply. Circuit A uses a p-type BJT (pnp) as transistor Q_1 . To keep the load disconnected from the power supply, the base voltage of Q_1 must be kept high. The base resistor determines the transistor base current (I_b) and should be sized to provide sufficient current above the amount required for the transistor to remain active [36].

Circuit B uses two BJTs to control the connection between the load and the power supply. The npn transistor Q_2 is in cutoff when its base voltage is low. This causes resistor R_3 to keep the base of pnp transistor Q_3 connected to the power supply, keeping Q_3 in cutoff. When the base voltage of Q_2 is increased, the npn transistor conducts. This connects the base of Q_3 to ground, causing Q_3 to conduct and connect the power supply to the load. Resistors R_1 and R_2 determine the base currents of the transistors. Resistor R_3 is only needed to keep Q_3 in cutoff, so its size is not important [36].

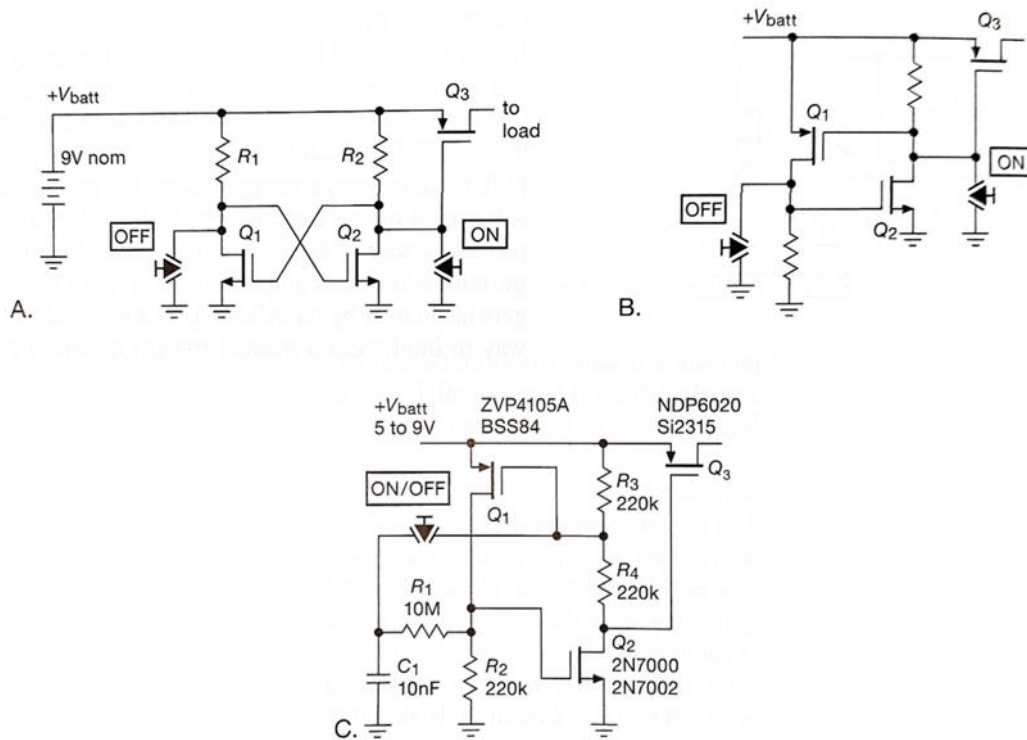


Figure 18: On/off battery control circuits implemented with MOSFET flip-flops [36]

Figure 18 presents three on/off battery control circuits implemented with MOSFETs. The basic idea is similar to circuit B in Figure 17, where the conduction of a transistor between a load and a power supply is regulated by another transistor. However, the circuits in Figure 18 include switches to turn the device on or off [36].

Circuit A uses a flip-flop circuit consisting of NMOS transistors Q_1 and Q_2 to control the conduction of PMOS transistor Q_3 placed between the battery and the load. The circuit employs two switches: one to turn the device on and one to turn it off, toggling the flip-flop between two states. When the off button is pressed, the gate voltage of Q_2 is connected to ground, putting the transistor in cutoff. The gate of Q_1 is connected to the battery power supply, causing it to conduct, and the gate of Q_3 is connected to the battery power, keeping it in cutoff. Even after the button is released, the transistors maintain this state because Q_1 keeps Q_2 in cutoff, which in turn keeps Q_3 in cutoff [36].

Pressing the on button toggles the flip-flop state. The gate of Q_3 is connected to ground, causing it to conduct and connect the battery to the load. The gate of Q_1 is also connected to ground, putting it in cutoff, which allows Q_2 to start conducting. The flip-flop maintains this state until interrupted [36].

The downside of this circuit is that it draws current in both the off and on states because one transistor in the flip-flop is always conducting. However,

the standby current can be minimised by using a large resistor for R_1 . Alternatively, the circuit can be redesigned to use a complementary flip-flop with one PMOS and one NMOS, as seen in circuit B of Figure 18, instead of using two transistors of the same type [36].

Circuit C of Figure 18 draws no current in the off state and uses a single button to toggle the flip-flop between on and off states. When the device is turned on, the gate of PMOS transistor Q_1 is connected to ground, causing it to conduct. This, in turn, connects the gate of NMOS transistor Q_2 to the battery power, causing Q_2 to conduct as well. Q_2 then connects the gate of Q_3 to ground, causing Q_3 to conduct and connect the battery to the load. In the on state, capacitor C_1 is connected to power and begins to charge. The flip-flop maintains the on state until the switch is pressed again [36].

When the button is pressed again, the device turns off. The capacitor releases its charge, powering the gate of Q_1 and causing Q_1 to stop conducting. Consequently, the gate of Q_2 is connected to ground, and Q_2 stops conducting. This allows the gate of transistor Q_3 to connect to the battery power, causing Q_3 to go into cutoff and disconnect the battery from the load [36].

While the operation of circuit C of Figure 18 is fairly simple, it involves several time constants. There are separate charging times for the capacitor across resistors R_1 and R_3 , and a discharge time for the output transistor's gate capacitance across resistors R_3 and R_4 . The charging time across R_1 should be slow to accommodate switch bounce, set in circuit C to 100ms. The charging time across R_3 should be shorter, set to 2ms, and the discharge time should be even faster, set to 0.4ms [36].

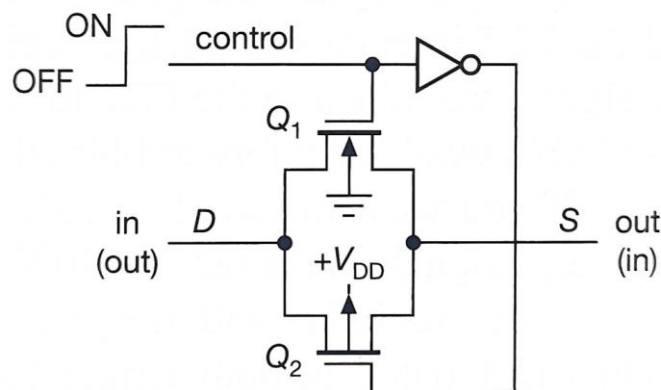


Figure 19: CMOS transmission gate [36]

Figure 19 presents a transistor switch circuit that is commonly available as an integrated circuit (IC), known as a transmission gate. The circuit consists of complementary MOSFETs, an NMOS and a PMOS, connected in parallel. When gate voltage of the NMOS transistor Q_1 is high, it conducts. Similarly, the PMOS transistor Q_2 conducts when its gate voltage is low. This configuration allows the circuit to operate bidirectionally, meaning either

terminal can serve as the input or output. An inverter is placed between the control signal and the gate of Q_2 to ensure that both transistors receive complementary signals. As a result, when the control signal is low, both transistors are turned off, and when it is high, both are turned on. Transmission gate ICs are available in a variety of configurations and voltage ranges [36].

The choice of circuit topology depends on the required functionalities of the device. The circuits shown in Figure 18 can both activate and deactivate the device, but they require more components, leading to increased power consumption, leakage current, and cost [36, 37]. Circuits can be designed using either BJTs or MOSFETs [36]. BJTs are typically less expensive but have higher leakage current and consume more power during operation. MOSFETs, the most commonly used transistors, have low leakage current and consume minimal power since they operate with voltage. However, while BJT leakage current remains relatively stable across temperatures, MOSFET leakage current increases exponentially with rising temperatures [36, 37]. The leakage current can be somewhat controlled by selecting specific BJTs or MOSFETs. MOSFETs with higher threshold voltage generally exhibit less leakage current [37]. Some BJTs are also optimised for low power dissipation and minimal leakage currents. The impedance of transistors in the active state varies as well. BJTs have higher impedance when active, whereas MOSFET impedance is lower but highly temperature dependent. Ultimately, the circuit's structure depends on the desired functionalities and priorities, whether they are functionality, low power consumption, stability, cost-effectiveness, or minimal leakage current [36, 37].

3 Methodology

This chapter outlines the experimental and simulation-based methods used to obtain the results discussed in Chapter 4. This thesis involved discharging zinc-air batteries under both constant and fluctuating current conditions to evaluate the impact of varying load profiles. Selected batteries were also intentionally aged prior to testing to assess the impact of aging on battery performance. Weight measurements of batteries were recorded before and after discharge to explore the correlation between changes in weight and discharge behaviour. A simulation-based approach was employed to estimate the equivalent circuit parameters of the batteries, while x-ray computed tomography (CT) imaging was used to analyse internal changes. Finally, simulations were conducted to evaluate the applicability of battery on/off control circuits in the context of a single-use clinical monitoring patch.

3.1 Discharge measurements with constant current

Size 13 zinc-air hearing aid battery cells from various manufacturers and conditions were subjected to a constant current discharge test. Each battery, with an initial voltage of approximately 1.3V, was connected in series with a 422Ω resistor, resulting in a discharge current of around 3mA. The battery voltage during discharge was continuously monitored using a PicoLog ADC-24 data logger, which was connected to a computer running Pico data logger software to capture the discharge curves. This test setup is described in Figure 20.

The batteries were connected to the ADC-24 terminal board via a custom-made testing board equipped with battery clips and resistors. To minimise interference, the entire test setup was securely mounted on a plastic board. The batteries were connected to the load within minutes of exposure to air, and the measurements were conducted at room temperature. The voltage data was logged continuously until the batteries were fully depleted. The recorded data was then processed using MATLAB.

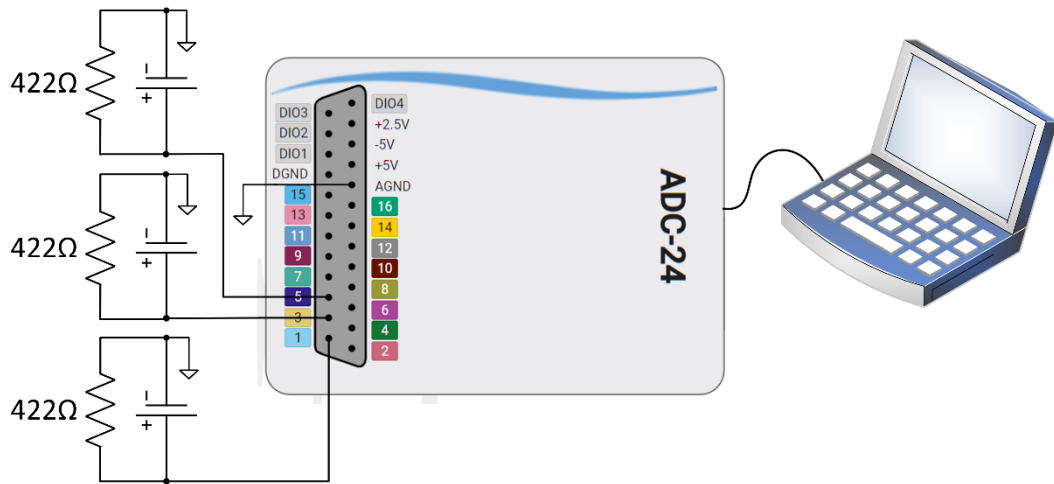


Figure 20: Test setup for constant current discharge tests

3.2 Discharge measurements with fluctuating current

Size 13 zinc-air hearing aid batteries from various manufacturers and conditions were subjected to a discharge test with periodically fluctuating current. The current had a period of 1 second with a nominal current of 3mA, but the peak amplitude and duty cycle were subject to change. Each battery was placed in a battery clip on a custom-made testing board. The test boards were secured together on a plastic platform to keep them in place, and each battery's positive and negative terminals were routed to a D25 sub connector. This setup is presented in Figure 21. The batteries were connected to the setup within minutes of exposure to air.



Figure 21: Battery setup for discharge tests with fluctuating current

The battery setup was connected via the D25 sub connector to a PXIe-4141 Source Measure Unit (SMU) in a National Instruments PXI system. The PXI system, controlled by a provided LabVIEW program, managed the current

profile of the batteries and measured their voltage. The LabVIEW program allowed for precise adjustment of the width and amplitude of current pulses and included a cutoff voltage feature, which stopped the measurement when all battery voltages dropped below a specified threshold. The LabVIEW program used can be found in Appendix A. The complete test setup is illustrated in Figure 22. The recorded data was processed using MATLAB.



Figure 22: The complete setup for discharge tests with fluctuating current

3.3 Shelf-life aging of batteries

To explore the effects of extended storage times on zinc-air batteries stored outside their original packaging, batteries were kept in various storage conditions for different durations. Each storage condition was considered as a potential option for storing clinical monitoring patches with zinc-air batteries after manufacturing. Therefore, each shelf-life battery sample was treated similarly to real-life conditions. The batteries were removed from their packaging and had the tabs covering the openings in the battery casing removed. They were then exposed to air for a few minutes, and stored in a bag or container as the finished product would be.

A total of 119 size 13 zinc-air hearing aid battery cells from two different manufacturers were tested. All batteries used had the same expiration date, June 2025, except for those placed in shelf-life testing in 2022. Among these, most had an expiration date of November 2024, while a few were marked for June 2025. This approach largely ensured consistency across the sample set. The start date of the shelf-life test was recorded, along with the battery manufacturer and the approximate time the battery spent in open air before storage. Storage methods included ESD bags, plastic zipper bags, and plastic containers, with separate test batches created annually for three years. All batteries, regardless of year and storage method, were stored in the same

location where temperature, humidity, and pressure were monitored. The battery shelf-life samples are listed in Table 1. Appendix B provides pictures and additional details of the storage methods used.

Table 1: Shelf-life aged battery samples

Start date	Manufacturer	Storage method	Number of samples
10-Apr-2024	Ansmann	ESD bag	6
10-Apr-2024	Energizer	ESD bag	8
10-Apr-2024	Ansmann	CPP/OPP laminated bag	6
10-Apr-2024	Energizer	CPP/OPP laminated bag	8
10-Apr-2024	Ansmann	Plastic container	3
10-Apr-2024	Ansmann	Original packaging	6
10-Apr-2024	Energizer	Original packaging	8
06-Mar-2023	Ansmann	ESD bag	9
06-Mar-2023	Ansmann	Plastic zipper bag	9
06-Mar-2023	Ansmann	Paper/plastic bag	6
06-Mar-2023	Ansmann	Original packaging	12
09-Mar-2022	Ansmann	Plastic container	12
09-Mar-2022	Ansmann	Acrylic container	3
09-Mar-2022	Ansmann	Original packaging	23

3.4 Equivalent circuit modelling and response time analysis

To investigate the relationship between the discharge behaviour of a zinc-air battery and its equivalent circuit components, a Thevenin equivalent circuit was modelled in Simulink and adapted to replicate the behaviour of a real zinc-air battery. The circuit structure, shown in Figure 11, was implemented in Simulink with all parameters defined and controlled from MATLAB. Parameters were passed from MATLAB to Simulink, and simulation outputs were returned to MATLAB for further analysis.

The model was subjected to the same fluctuating current profile used in the discharge of the real zinc-air battery to ensure a meaningful comparison. The fluctuating current profile is necessary to induce transient behaviour, allowing the dynamic response of the circuit and thus the response time to be observed. Simulations were run over 10-second intervals, and the output voltage of the equivalent circuit was compared to the measured voltage of the real battery. Circuit parameters were manually adjusted to align the simulated output with the measured data. This fitting was repeated at 10% state-of-charge intervals along the entire discharge process to capture how the equivalent circuit components evolved as the battery depleted.

3.5 Battery weight measurements

Before each discharge test, the battery cells were removed from their packaging and exposed to air. Their weight was measured using a Mettler Toledo PB303-S high precision scale, which is shown in Figure 23. It has a readability of 0.001g and is calibrated annually to ensure accuracy.

After each discharge test, the battery cells were weighed immediately after being removed from the test setup. In cases where the battery leaked electrolyte during discharge, some inaccuracy was introduced due to the resulting weight loss. All weight measurements were conducted at room temperature.



Figure 23: Scale used in battery weight measurements

3.6 Investigation of battery aging through x-ray computed tomography

To evaluate the impact of aging on the internal structure of zinc-air batteries, x-ray computed tomography imaging was performed on a range of battery samples. These included six new size 13 zinc-air hearing aid batteries, two fully discharged to 0%, two partially discharged to 50%, and two left unused. In addition, 26 shelf-life aged samples were analysed from the study described in Chapter 3.3. These samples were collected from various storage conditions, with two batteries per manufacturer selected from each method and storage year.

To prepare the batteries for transport and imaging, they were removed from their storage environments and sealed with Kapton tape. The tape was used to cover the openings in the battery casings, minimising exposure to ambient air. This precaution ensured that any degradation observed during imaging could be attributed to the storage conditions rather than to handling.

Imaging was conducted using a Phoenix Nanotom x-ray computed tomography system with an operating voltage of 100kV, a current of 140 μ A, and a 0.5mm copper filter. The scan included 1200 projections, each with an exposure time of 1.5 seconds, and achieved a voxel size of 15 μ m. Two to three batteries were scanned simultaneously. The resulting images were analysed using the Fiji distribution of the ImageJ software.

3.7 Simulation of on/off battery control circuits

To evaluate the applicability of various on/off battery control circuit solutions for a single-use clinical monitoring patch, simulations were conducted in LTspice to analyse both circuit functionality and leakage currents. The relevant circuit topologies and design considerations are introduced in Chapter 2.4.3.

The simulations were performed as transient analyses over a 15-second period to capture the behaviour of the circuits. Each circuit was tested in its active state across a range of input voltages, starting at 3.75V from three unused zinc-air batteries in series and continuing down to the undervoltage lockout threshold of 1.8V. This ensured that the circuits remained operational throughout the expected battery discharge range.

The circuits were also simulated in their intended off-state to assess leakage currents, which indicate the current drawn from the battery when the device is not in use. Minimising this leakage is critical for maximising battery life in single-use applications.

To explore the impact of component selection, various transistor options were evaluated to understand their impact on circuit performance and leakage characteristics. Transistors were selected based on both retail availability and the existence of compatible LTspice models, including those sourced from online component distributors. This ensured that the components were not only suitable for simulation but also cost-effective and practical for real-world implementation.

4 Results and discussion

This chapter presents the results obtained through the experimental methods outlined in Chapter 3. Chapter 4.1 examines the effects of different current profiles and aging on zinc-air battery performance, based on measured discharge curves. Chapter 4.2 explores variations in battery lifetime in relation to parameters such as weight change, CT imaging data, and equivalent circuit components. Finally, Chapter 4.3 discusses the outcomes of simulations assessing battery on/off control circuits, with a focus on their applicability in the single-use clinical monitoring patch.

4.1 Impact of discharge conditions and aging on battery lifespan

4.1.1 Discharge with constant current

The single-use wireless monitoring patch consumes approximately 3mA of current. The impact of a 3mA constant current profile on battery lifespan was evaluated using 10 battery samples from two different manufacturers. The batteries from both manufacturers are practically identical, except Varta batteries have three holes in the casing, while Energizer batteries have two. All discharged batteries were brand new and had more than three years remaining until their expiration date. The discharge curves of the 10 discharged batteries are presented in Figure 24.

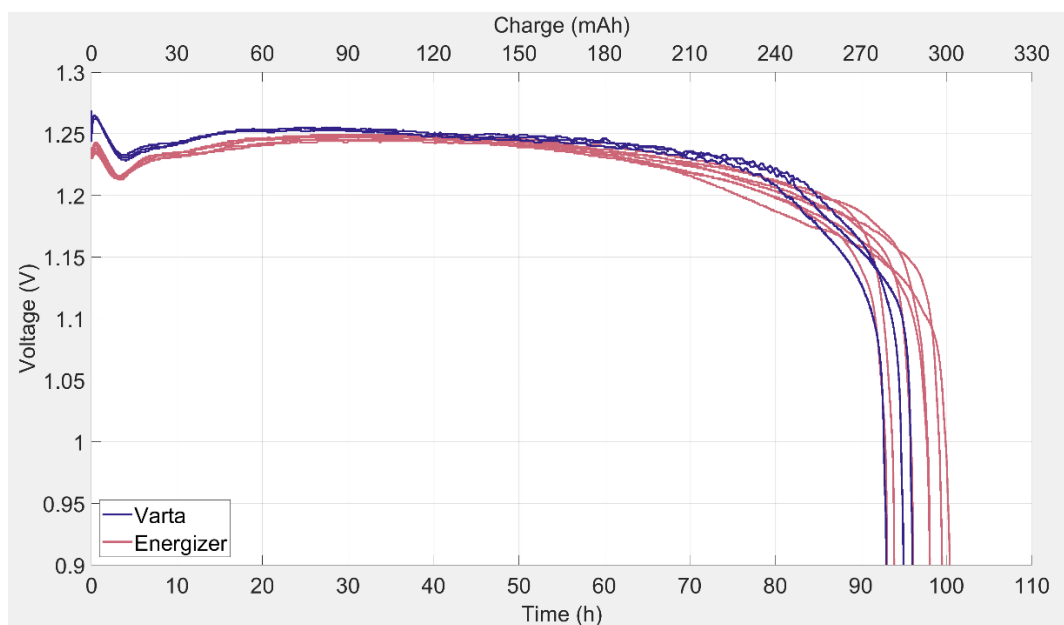


Figure 24: The discharge curves of brand-new zinc-air battery cells with a constant discharge current of 3mA

Figure 24 displays the measured voltage of each battery over time and in relation to the state of charge. The capacity was calculated by multiplying the discharge current value (3mA) with the elapsed number of hours. Figure 24 shows the typical characteristics of a zinc-air battery discharge curve. At the beginning of the discharge process, the curves show a voltage dip at a capacity of approximately 8mAh, or a relative capacity of 3%, for each battery. After the voltage dip, all batteries stabilize to approximately 1.25V during the plateau phase. This corresponds to a maximum input voltage of 3.75V for the single-use clinical monitoring patch, which is powered by three zinc-air batteries connected in series. The plateau phase lasts an average of 2 to 3 days before the onset of the last voltage decline. The steep voltage decline continues until the battery cutoff voltage is reached, which was set to 0.9V. On average, the batteries had a lifetime of 96.3 hours and a capacity of 289mAh.

Given the minimal variation in the location of the voltage dip among individual batteries, it can be concluded that the batteries have undergone little aging or self-discharge, consistent with their new condition. However, a clear correlation between the voltage level of the dip and the battery manufacturer can be observed. Energizer batteries start at a lower voltage level than Varta batteries. This difference could be explained by the varying number of openings in the battery casing, with Varta batteries reaching equilibrium for the oxygen reduction reaction faster than Energizer batteries, which have a reduced oxygen intake. During the plateau phase, Varta batteries stabilize at a marginally higher voltage level, indicating they likely have a slightly lower internal resistance. A clear difference between manufacturers is again seen during the voltage decline, with Varta batteries having a shorter lifetime and a steeper voltage decline, while Energizer batteries have a somewhat longer lifetime and a gentler slope in the decline. Thus, Varta batteries maintain a higher voltage for longer, but Energizer batteries have a longer overall lifetime. According to the manufacturer Energizer batteries have a typical capacity of 285mAh with a 1.05V cutoff [38]. In the figure we can see that Energizer batteries are usually above this value, while Varta batteries are a bit below it.

These findings highlight the predictable behaviour of new batteries when discharged with a constant current, revealing distinct manufacturer-specific characteristics. However, it is important to note that these discharge curves were obtained under highly controlled conditions. In practical applications, the current consumption will vary, and batteries will not always be brand new. Additionally, external factors such as temperature, humidity, and device usage patterns will influence the discharge process.

4.1.2 Discharge with fluctuating current

A total of 40 size 13 zinc-air hearing aid battery cells were tested by discharging them with fluctuating discharge currents. The current alternated between

a low and a high current level with a specific frequency and duty cycle, the related terminology is illustrated in Figure 25. Duty cycle refers to the relative portion of time spent at the higher current level. The fluctuating current had a frequency of 1Hz and a nominal current of 3mA. However, the duty cycle and the high and low current values varied with each measurement to assess their impact on battery discharge behaviour and lifespan. Each measurement included between two and four battery samples from the manufacturers Energizer and Varta. All batteries were new and had more than three years remaining until their expiration date. Figure 26 illustrates the resulting measurements.

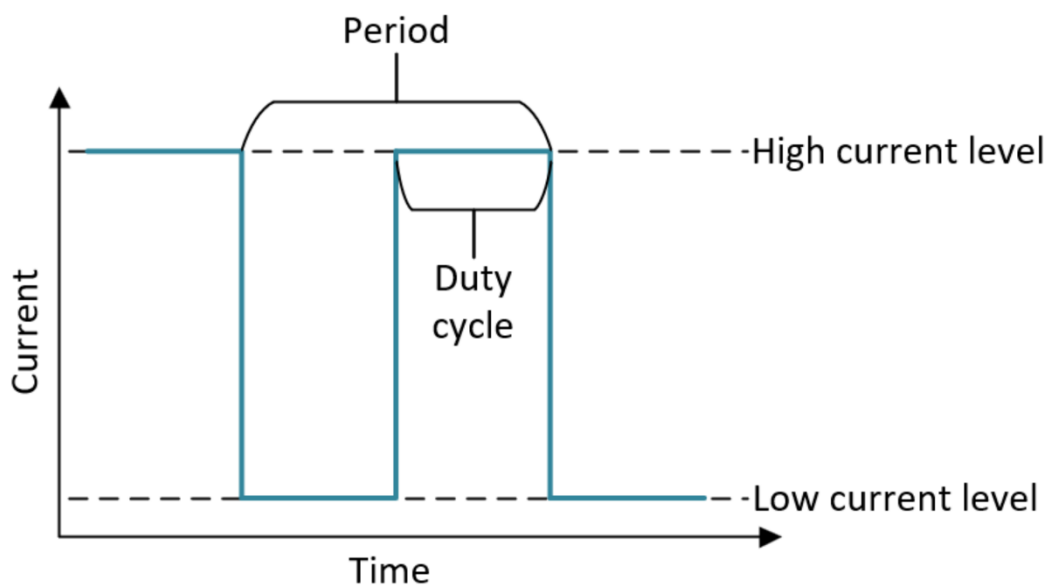


Figure 25: Illustration of fluctuating current terminology, including duty cycle, period, high current level and low current level

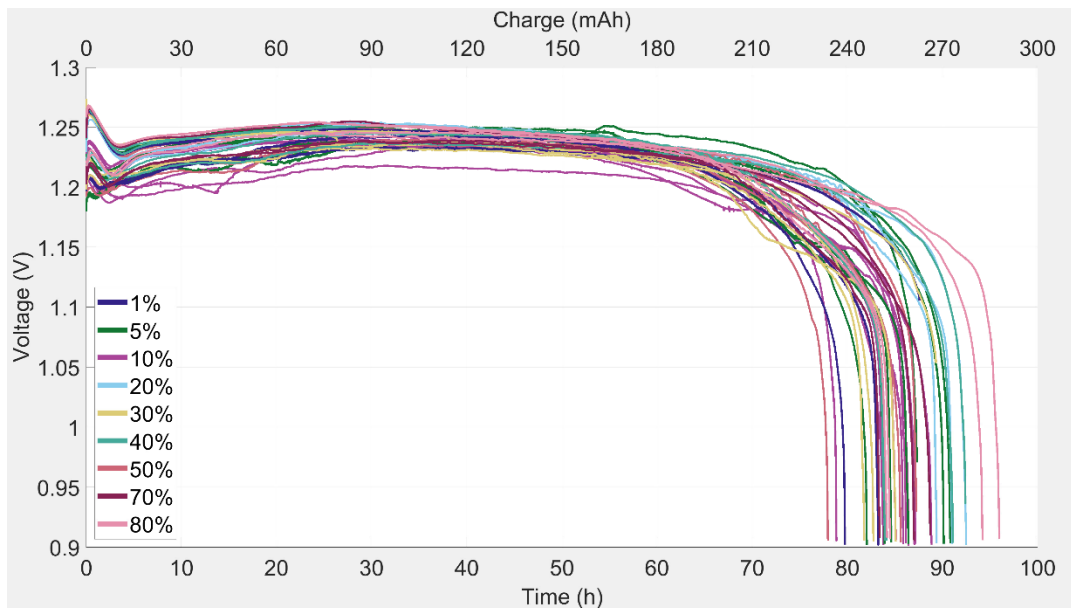


Figure 26: Discharge curves of batteries discharged with fluctuating currents with a frequency of 1Hz and nominal current of 3mA

Figure 26 displays the voltage of each battery over time and in relation to the state of charge. The colour of each discharge curve represents the duty cycle of that battery's discharge current. The voltage of each curve is the average of the measured fluctuating voltage, allowing the typical characteristics of the discharge curves to be observed. Each battery voltage exhibits an initial voltage dip, even under fluctuating discharge currents. However, there is greater variation in the depth and location of the dip between individual batteries compared to those with a constant discharge current seen in Figure 24. The plateau phase shows more variation in voltage level and duration, along with unexplained dips and peaks. Nevertheless, the batteries eventually stabilise to approximately the same voltage level as those discharged with constant current. The plateau phase is followed by a rapid voltage decline, indicating the battery is depleted.

The batteries with fluctuating discharge currents also exhibit more variation in lifetime between individual units compared to those with constant discharge currents. The variation in battery lifetimes is approximately 15 hours for fluctuating currents, versus 10 hours for constant currents. Some variation is expected due to the larger sample size and the use of drastically different current profiles. However, the batteries with shorter lifetimes tend to experience their initial voltage dip earlier than anticipated. Since the voltage dip is expected to occur at the same relative capacity for each battery, it can be inferred that some batteries discharged faster than others, likely due to their specific current profiles.

On average, batteries discharged with fluctuating current had a lifespan of 85 hours and a capacity of 255mAh. This is approximately 12% lower than the average lifetime of batteries discharged with constant current, and 10.5% lower than the typical capacity indicated in the Energizer battery datasheet [38]. While some batteries discharged faster due to their current profiles, others with fluctuating current experienced voltage dips at the same relative capacity as those with constant current. However, their overall lifespans remained shorter than those discharged with constant current. This indicates that, although the current profile can accelerate discharge, the lifespan is also inherently limited by the battery running out of usable material when discharged with fluctuating current.

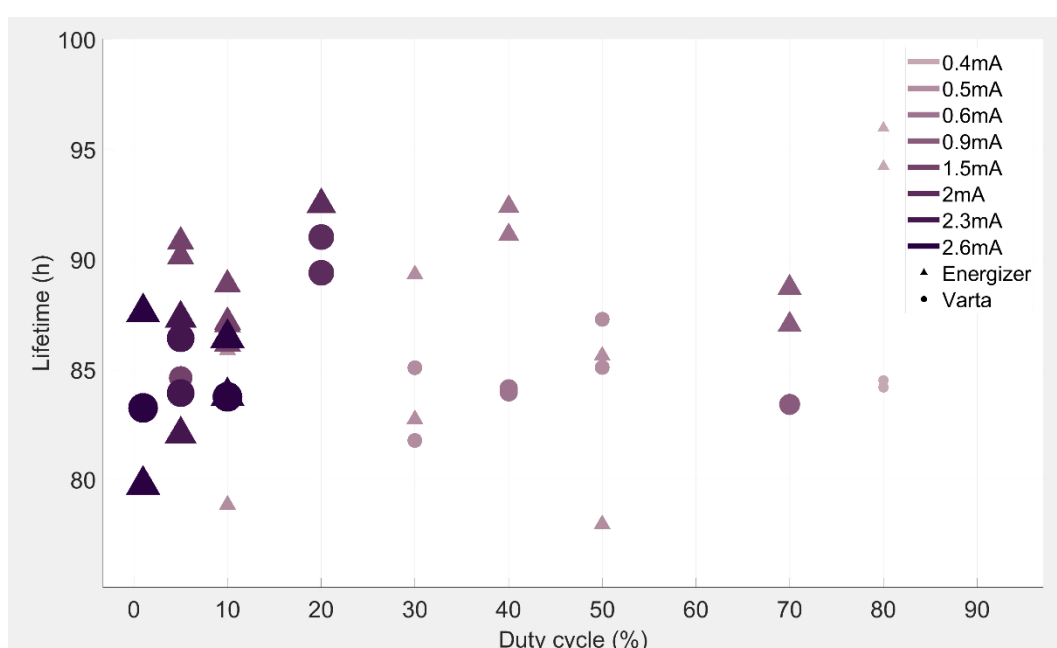


Figure 27: Duty cycle and lifetime of batteries discharged with fluctuating current with low-level current represented by colour and size of the marker

Figure 27 presents a scatter plot of battery samples discharged under fluctuating current conditions, comparing their lifespan to the duty cycle of the applied current. The colour and size of each marker represent the low current level, while the shape indicates the battery manufacturer. The relationship between duty cycle and battery lifespan appears to follow a roughly cubic trend. As the duty cycle increases from 0%, the lifespan initially increases, peaking at 20%. Beyond this point, the lifespan decreases, reaching a minimum at 50%. Above 50%, the lifetime increases rapidly again. This upward trend appears to approach the maximum values previously observed at a 100% duty cycle, as shown in Figure 24.

Since each current profile maintains an average current of 3mA, a smaller duty cycle generally corresponds to a higher low current level. In addition, a

decrease in low current level necessitates an increase in the high current level. At duty cycles where multiple low current levels were tested, batteries exposed to lower low- level currents tended to exhibit longer lifespans.

Notably, the 2mA low current level at a 20% duty cycle resulted in the longest lifespan observed below 50%. Beyond 50%, the lifespan continued to increase until reaching its maximum at 100% duty cycle under a constant current of 3mA. Regarding battery manufacturers, while the difference in lifespan is not substantial, Energizer batteries tended to have longer lifetimes compared to Varta batteries. This distinction is particularly clear at duty cycles of 40%, 70%, and 80%, as shown in Figure 27.

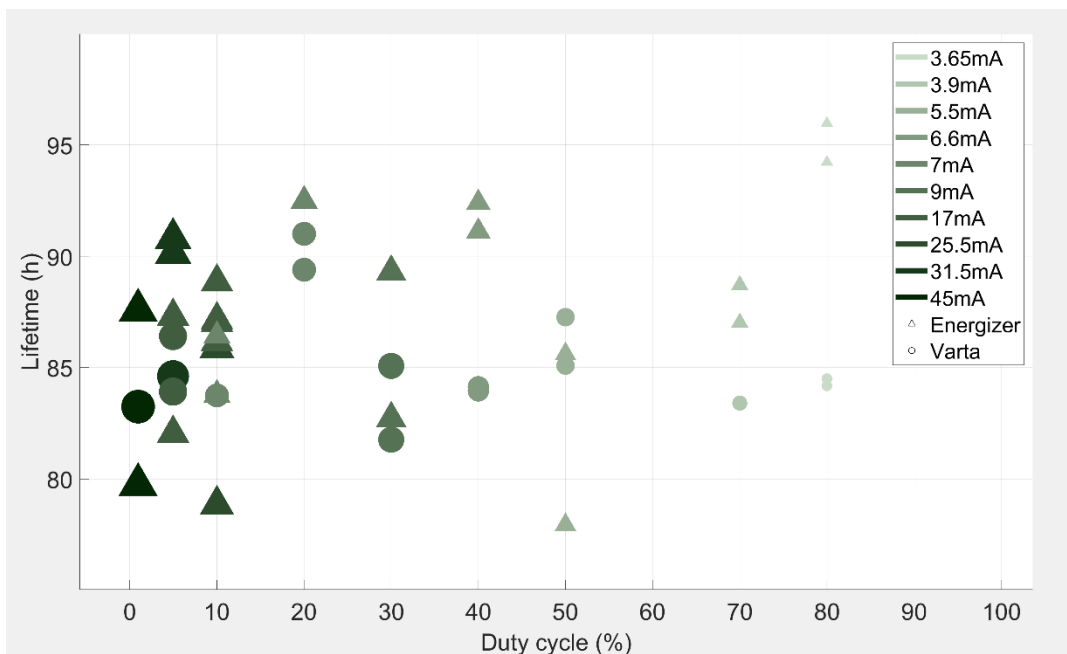


Figure 28: Duty cycle and lifetime of batteries discharged with fluctuating current with high-level current represented by colour and size of the marker

Figure 28 presents a scatter plot of battery samples discharged with fluctuating current, comparing their lifespan and the duty cycle of the current. The colour and size of each marker represent the high current level, while the shape indicates the battery manufacturer. When compared to Figure 27, it is evident that lower low current levels correlate with higher high current levels at the same duty cycle, due to the fixed average current of 3mA. Therefore, as implied in Figure 27, higher currents at the same duty cycle in Figure 28 correlate with longer lifetimes. This makes it difficult to conclude whether the low current level or high current level specifically affects lifespan. Beyond this, there is no clear correlation between high current level and battery lifespan. The batteries can tolerate current pulses of over 45mA without substantial impact on lifespan, and very low currents can result in lifetimes both above and below average.

Based on these results, it is difficult to determine battery lifetime solely based on duty cycle, low current level, or high current level. This contrasts significantly with lithium-ion batteries, which exhibit a predictable relationship between duty cycle and lifetime, as shown in Figure 10. For zinc-air batteries, the lifetime is likely influenced by a complex combination of all three factors. The lifetime in relation to fluctuating current seems to depend on finding a balance where current peaks are low enough to avoid excessive damage, the duty cycle is large enough to keep the current low but small enough to allow the battery to recover between peaks, and the low-level current is sufficiently low to enable effective recovery. In these measurements, high current peaks did not appear to cause notable damage, likely because they were adjusted to be brief.

In these measurements, batteries with a 20% duty cycle, a low-level current of 2mA, and a high-level current of 7mA had the longest lifetime below a 50% duty cycle. These batteries had an average lifetime of over 90 hours, which is comparable to the constant current samples. However, further exploration of different current profiles with varying combinations of duty cycle, low current level, and high current level is needed to identify potentially better combinations. Despite this, Figure 27 and Figure 28 confirm that constant current discharge is the most ideal current profile for zinc-air batteries.

4.1.3 Discharge of aged batteries

The influence of age and different storage methods on battery lifetime was investigated by discharging intentionally aged size 13 zinc-air hearing aid battery cells from various manufacturers. The shelf-life aged batteries that were stored in different ways to explore the impact of storage methods are detailed in Chapter 3.3. Shelf-life aged batteries were discharged with a constant current of 3mA.

Other aged battery samples from Ansmann, Varta, and Energizer were stored in their original packaging with the tab covering the openings in the battery casing. At the time of discharge, the Varta and Ansmann batteries were 4 months from expiration, while the Energizer batteries were 1 year away. Both the Ansmann and Energizer batteries had 4 openings in their casing, whereas the Varta batteries had 3 openings. The batteries stored in original packaging were discharged either with fluctuating current at a frequency of 1Hz and a nominal current of 3mA, or with a constant current.

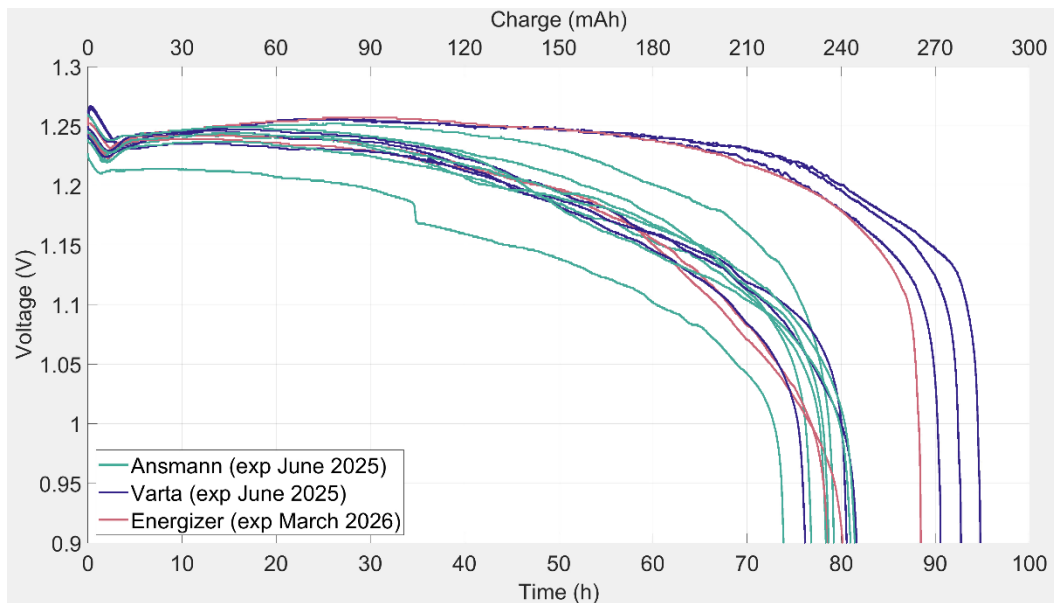


Figure 29: Batteries aged in original packaging discharged with a constant current of 3mA

Figure 29 presents the discharge curves of batteries aged in their original packaging and discharged with a constant current. The typical characteristics of a zinc-air battery discharge curve are evident in the figure. Interestingly, the location and depth of the initial voltage dip are consistent with the new batteries shown in Figure 24, indicating minimal self-discharge. During the voltage plateau phase, the batteries separate into two distinct groups, some maintain a higher voltage level similar to the new batteries, while others exhibit a declining voltage throughout most of their lifetime. Following the plateau phase, some batteries, particularly those in the lower voltage group, display distinct voltage steps not typically seen in new batteries. The discharge concludes with a sudden voltage drop, indicating depletion.

The division during the plateau phase results in two distinct groups based on their lifetime: the higher group averages over 90 hours, while the lower group averages 78 hours. The higher group is comparable to new batteries, whereas the lower group has declined in lifetime by over 10 hours. This suggests that aging causes batteries to step down from the upper to the lower level, potentially due to corrosion or loss of water. This could render zinc with lower activation energy unusable or increase internal resistance. Consequently, the corrosion could reach a point where the battery cannot maintain its voltage level, leading to a decreased lifetime. This division appears to correlate with the manufacturer, as all Ansmann batteries fall into the lower lifetime group, while Energizer and Varta batteries are evenly split between the two levels. The Energizer batteries are newer than the Varta ones, suggesting that the Varta batteries have aged the slowest.

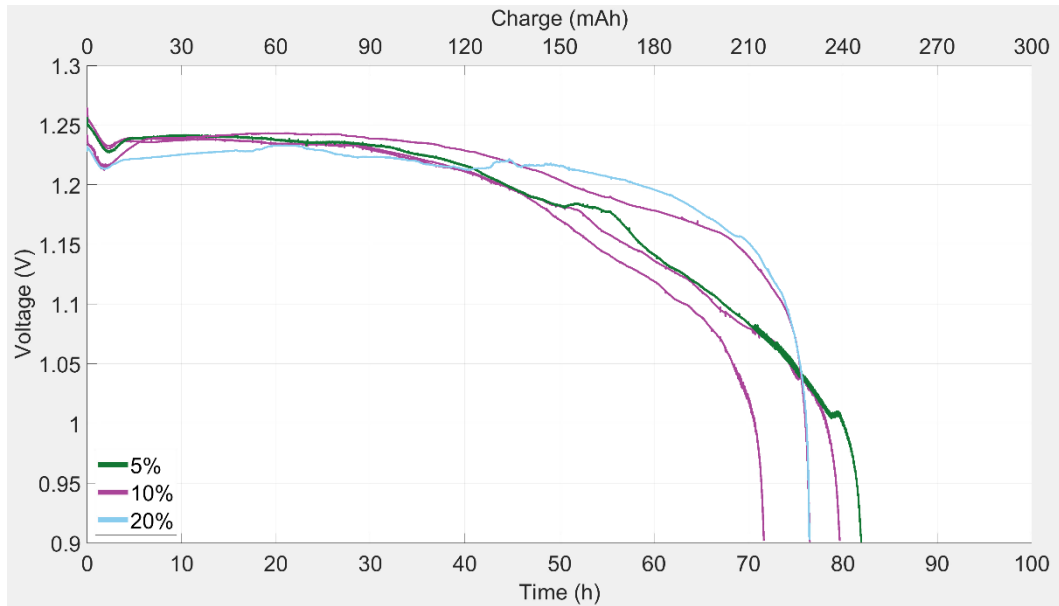


Figure 30: Batteries aged in original packaging discharged with fluctuating currents with a frequency of 1Hz and a nominal current of 3mA

Figure 30 shows the discharge curves of batteries aged in their original packaging and discharged with fluctuating currents at a frequency of 1Hz and a nominal current of 3mA. All discharged batteries were from Ansmann, expiring in June 2025. The measured fluctuating voltage was averaged in the figure to make the discharge curve characteristics visible. The colour of each battery discharge curve reflects the duty cycle of its discharge current. In Figure 27, it was evident that a duty cycle of 20% resulted in the longest lifetime of any duty cycle below 50%. However, this is not the case in Figure 30. This suggests that either aging or the manufacturer impacts how different current profiles compare in terms of lifetime. Since these batteries are all from Ansmann, it can be assumed that if the same division exists in Figure 30 as in Figure 29, all batteries are in the lower lifetime group. Interestingly, when comparing the lifetimes of the lower group in Figure 29 with the average lifetime in Figure 30, there is no change. This contradicts the results for new batteries, where those discharged with constant current in Figure 24 always had a longer lifetime than those discharged with fluctuating current in Figure 26. Aging clearly affects how the battery tolerates fluctuating currents.

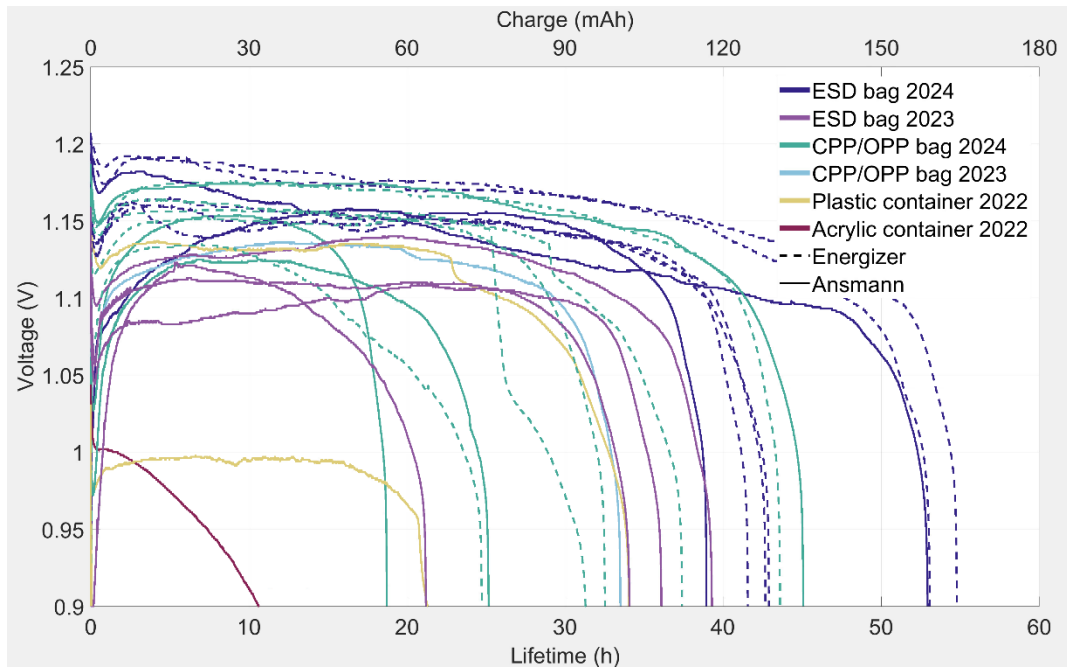


Figure 31: Discharge curves of shelf-life aged batteries with a constant discharge current of 3mA

Figure 31 presents the discharge curves of shelf-life aged batteries discharged with a constant current of 3mA. Despite significant aging, the figure exhibits the expected characteristics of zinc-air battery discharge curves. The location and depth of the initial voltage dip vary considerably, occurring much earlier than in new batteries shown in Figure 24. This suggests a decreased capacity from the start, likely due to self-discharge or corrosion. The voltage dip also appears deeper in batteries with shorter lifetimes, indicating they require more energy to reach the initial equilibrium of internal reactions. Following the voltage dip is the plateau phase, where the length and voltage level vary significantly between individual batteries. A lower voltage level, indicating higher internal resistance, seems to roughly correlate with shorter lifetimes and is therefore likely caused by corrosion. Some batteries also exhibit voltage steps after the plateau phase, indicating a switch to consuming zinc with higher activation energy. These voltage steps are most visible in batteries with longer lifetimes, probably because batteries with shorter lifetimes no longer had material with another activation energy level to switch to. The discharge curves all conclude with the final voltage decline.

While attempts were made to discharge all shelf-life aged batteries, only those shown in Figure 31 were successfully activated. These included batteries stored in electrostatic discharge (ESD) bags for 1 and 2 years, as well as those stored in CPP/OPP (cast polypropylene/oriented polypropylene) laminated bags for 1 year. Additionally, individual batteries stored in CPP/OPP bags for 2 years, in plastic containers for 3 years, and in acrylic containers for

3 years were also successfully activated. Notably, a battery stored in a plastic container since 2024 showed potential. However, the sample size was limited to three batteries. Of these, two were used in CT imaging, leaving only one for discharge testing. Unfortunately, data logging failed during this test, so no discharge curve was recorded, and the result is therefore not included in Figure 31. Nevertheless, this battery that was stored in a plastic container for 1 year was estimated to have a lifetime of 56 hours, which is the longest observed lifetime among all shelf-life aged batteries.

Typically, batteries stored in ESD bags had the longest lifetimes, and as expected, newer batteries had longer lifetimes than older ones. Energizer batteries also generally had longer lifetimes than Ansmann batteries. Regardless, removing the batteries from their original packaging significantly impacts their lifetime. The best battery lifetime in Figure 31 was 55 hours, compared to Energizer batteries with the same expiration date stored in their original packaging in Figure 29, which had lifetimes between 80 and 90 hours. Despite this reduction in lifetime, these results still suggest that it is possible to store zinc-air batteries outside their original packaging for extended periods, which is necessary for the single-use clinical monitoring patch.

Not only does aging significantly impact the lifespan of zinc-air batteries, especially those stored outside their original packaging, but it also makes their behaviour during depletion much less predictable. Aged batteries exhibit varying lifetimes and voltage levels, and the behavioural patterns observed in new batteries do not seem to apply. Therefore, it is crucial to maintain batteries in conditions that preserve their new-like behaviour through optimal storage methods.

4.2 Methods of estimating state of charge

4.2.1 Coulomb counting

The applicability of using coulomb counting to monitor the state of charge in zinc-air batteries can be evaluated based on the measured discharge curves in this thesis. This evaluation allows for assessing how suitable coulomb counting is for size 13 zinc-air hearing aid battery cells from various manufacturers, with different discharge current profiles and ages. Coulomb counting involves knowing the initial and final capacity of the battery and tracking the amount of capacity consumed between these points. Therefore, for coulomb counting to be applicable, these capacity values need to be as predictable as possible. The less predictable the battery's lifetime, the more likely the coulomb counter is to inaccurately predict when the battery is depleted. This can result in either promising too long a lifespan and failing to warn of depletion or warning too early and wasting battery capacity.

In Figure 24, new zinc-air batteries were discharged with a constant current of 3mA. This current profile provides the longest and most predictable lifetimes, making it the ideal discharge current profile for zinc-air batteries in this thesis. The start capacity for new batteries is very predictable. Due to the lack of aging, the batteries can be assumed to start at 100% capacity. Once depleted, there is approximately a 10-hour difference between the longest and shortest lifetimes. This variation can be reduced by using batteries from a single manufacturer. In Figure 24, Varta batteries show less variability in lifetime between individual cells compared to Energizer, with the difference between the longest and shortest lifetimes reduced to approximately 5 hours. If the coulomb counter were to assume the shortest battery lifetime, it would at most waste 5 hours of battery lifetime, which is minimal.

When new zinc-air batteries are discharged with a fluctuating current at a frequency of 1Hz and a nominal current of 3mA, as shown in Figure 26, the difference in lifetime between the longest and shortest increases to 15 hours. This includes a variety of brands and different current profiles. Using batteries from one manufacturer with one current profile results in a difference ranging from 3 to 10 hours, depending on the current profile. However, the sample size for each current profile is so small that it is uncertain whether the variation would be larger in reality. For new batteries, it can still be assumed they start at 100% capacity, but it becomes clear that for the lifetime to remain predictable, the current profile also needs to be consistent.

For aged batteries, the lifetime becomes less predictable as it can no longer be assumed that the batteries start at 100% capacity. In Figure 29, a clear step down in lifetime is observed as batteries age in their original packaging. There is no way of knowing exactly when this step down occurs, so if the coulomb counter assumes the battery behaves like a new one, it could be off by over 10 hours. The best approach is to choose a battery that ages the slowest, which in Figure 29 appears to be the Varta batteries, although even these eventually step down. However, in Figure 30, fluctuating current does not affect the lifetime of the stepped down batteries, which increases the predictability of their lifetimes.

For the shelf-life aged batteries in Figure 31, the lifespan varied by days between individual batteries. Even with a specific storage method, if the length of time the battery spends in storage is not considered, predicting the lifetime becomes almost impossible. The options are to find a storage method that better limits aging or to shorten the shelf-life time to make the lifetime easier to predict.

The primary challenge in making coulomb counting a reliable option for tracking the state of charge in zinc-air batteries is their aging process. Until the effects of aging can be limited or accounted for in the coulomb counter, it does not seem like a viable option for tracking the battery lifetime in single-use clinical monitoring patches. However, in theory, if the production process and storage conditions are made highly consistent, it could be possible

with enough data to develop a model that predicts how the lifetime decreases as zinc-air batteries age. Such a model could enable the device to estimate a battery's expected lifetime upon activation, based on its assembly date.

4.2.2 Equivalent circuit modelling and response time analysis

To investigate the relationship between the equivalent circuit components of a zinc-air battery and its state of charge, a simulation of the equivalent circuit was conducted. The circuit parameters were adjusted so that the simulated output voltage closely matched real voltage measurements from a discharging battery. To accurately estimate all circuit components, including those modelling transient behaviour, a fluctuating discharge current was required. For this purpose, an Energizer battery subjected to a discharge current with a 50% duty cycle, a high current level of 5.5mA, and a low current level of 0.5mA was used as the reference for adapting the circuit model. The equivalent circuit was simulated using the same current profile. The 50% duty cycle ensured that both the rising and falling edges of the fluctuating output voltage were as clearly defined as possible, which is essential for capturing transient dynamics. The discharge curve of this battery is shown in Figure 32. The effect of this current profile on the battery's lifetime was previously discussed in Chapter 4.1.2.

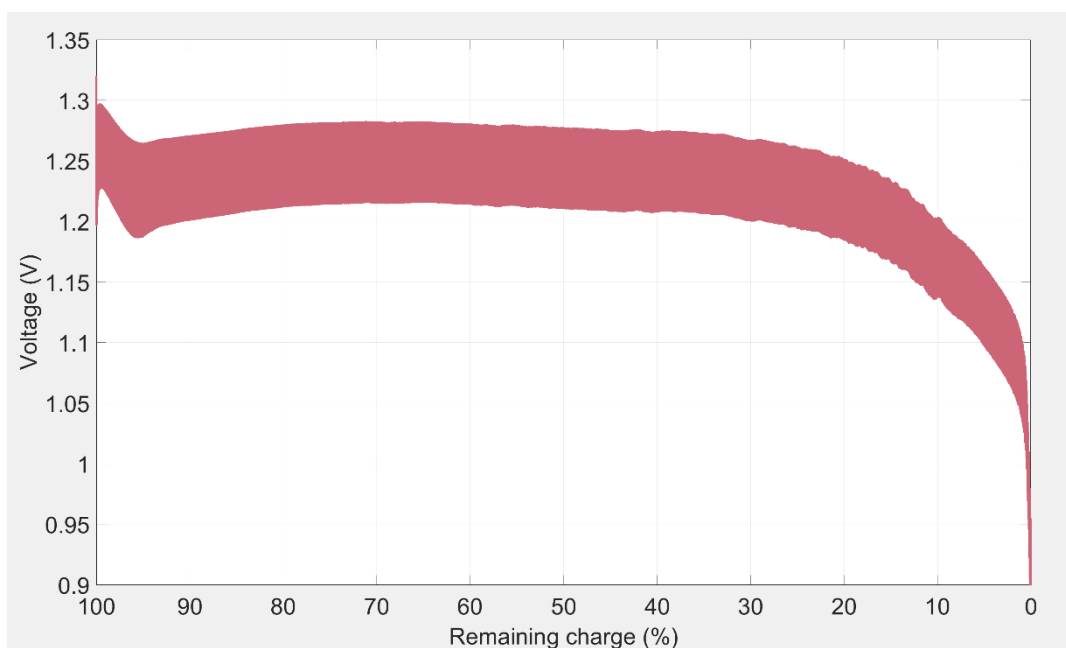


Figure 32: Discharge curve of a size 13 Energizer zinc-air hearing aid battery subjected to a fluctuating current with a 50% duty cycle. The current alternated between 5.5mA and 0.5mA at a frequency of 1Hz.

The equivalent circuit parameters were adapted to match the discharge curve in 10-second intervals, conducted at 10% steps from full charge to complete discharge. During this process, the open-circuit voltage, internal resistance, capacitance, and its parallel resistance were individually adjusted to ensure that the simulated output voltage closely followed the real discharge voltage of the zinc-air battery. How these circuit components form the equivalent circuit can be seen in Figure 11. Each of these parameters influenced the voltage curve in a distinct way. The open-circuit voltage established the overall voltage level, while the internal resistance affected the height of the voltage peaks. The capacitance and its parallel resistance shaped the slope at the top of each peak, reflecting the capacitor's charging behaviour. Since the battery's response time, governed by these two components as described in Equation 8, is known to correlate with the state of charge, particular attention was paid to accurately modelling the curvature of the voltage peaks.

Figure 33 presents the adapted result at 70% state of charge, where the equivalent circuit output closely aligns with the real discharge curve. This fitting process was repeated for each 10% step, and the complete set of results is available in Appendix C. Although the measured voltage data has limited resolution, which can make the simulated signal appear less accurate than it truly is, the circuit was tuned to align with the most clearly defined peaks in the measured voltage.

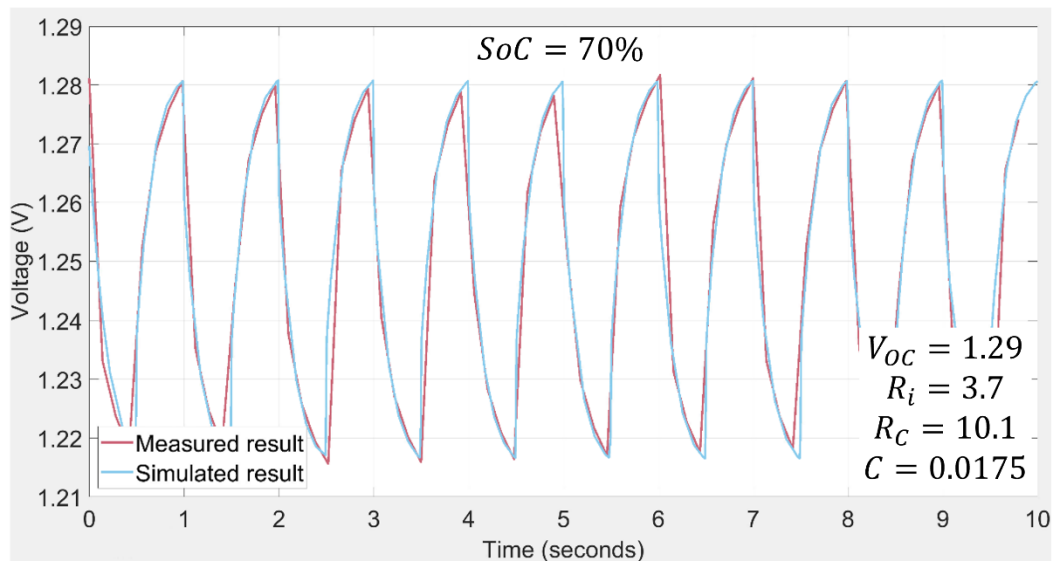


Figure 33: The output voltage of the zinc-air battery at 70% state of charge and the output voltage of the equivalent circuit with $V_{OC}=1.29$, $R_i=3.7$, $R_C=10.1$, and $C=0.0175$

The component values that produced the best fitting output voltages for the equivalent circuit over the battery's lifetime are shown in Figure 34. The open-circuit voltage (V_{OC}) follows the typical pattern observed in zinc-air battery discharge curves. It remains steady at approximately 1.3V for most of the

battery's life, followed by a sharp drop at the end. This open-circuit voltage is higher than the measured output voltage of a battery during discharge, as it is not affected by internal resistance. The internal resistance (R_i) generally decreases as the state of charge decreases. In contrast, the capacitance (C) and its parallel resistance (R_C) tend to increase with decreasing charge. The greatest variation in parameter values appears at the beginning of the discharge process, where the battery still holds most of its charge. This may be attributed to the initial voltage dip commonly observed in zinc-air battery discharge curves, which show a typical behaviour early into the battery's depletion. Notably, both R_i and the capacitance are unusually high at the start of the discharge compared to their values later in the process, while R_C only exhibits a dip at the 80% mark.

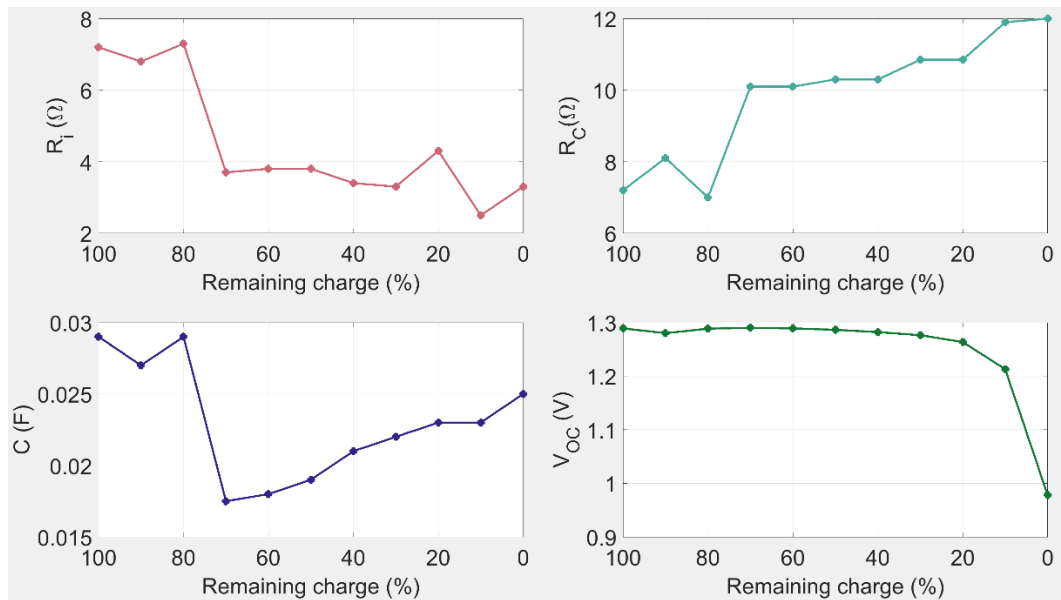


Figure 34: The equivalent circuit parameters determined through simulation

The response time (τ) of the equivalent circuit's output voltage is calculated as the product of the capacitance and its parallel resistance. Figure 35 shows how this response time evolves over the battery's lifetime. Generally, the response time tends to increase as the battery is depleted. However, the minimum response time occurs at around 70% state of charge, with a slight increase observed early in the battery's life. This early behaviour may be due to the equivalent circuit's inability to fully capture the initial voltage dip, which could distort the fitted parameter values. Alternatively, the voltage dip might influence the battery's capacitive properties. Since the dip is associated with a reduced number of charge carriers, and a lower carrier concentration can lead to increased capacitance, this explanation aligns with the observed result.

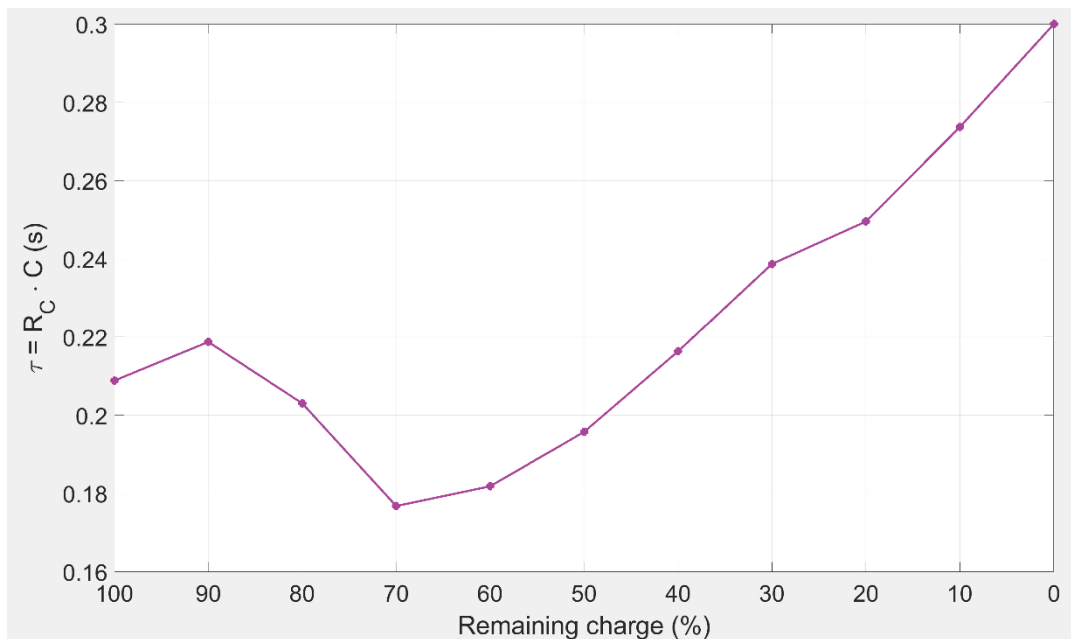


Figure 35: The response time of the equivalent circuit calculated across the battery's lifetime

The results regarding the component values of the equivalent circuit show only partial consistency with findings from other studies discussed in Chapter 2.3.4 and Chapter 2.4.2. In Figure 7, the relationship between the state of charge and the response time was described as exponential, which contrasts with the trend observed in Figure 35. However, the measurement in Figure 7 was conducted on a larger zinc-air battery and used a different current profile, with a period lasting several minutes rather than one second. These differences in battery size and current profile could significantly influence the relationship between the voltage response time and the state of charge.

Figure 12 illustrates how the equivalent circuit resistor values vary with the state of charge. There, the internal resistance exhibited a negative quadratic relationship with the state of charge, while the parallel resistance increased linearly as the battery discharged. In contrast, Figure 34 shows that the parallel resistance maintains a roughly linear trend, but the internal resistance does not follow a quadratic pattern. It is important to note that the measurements in Figure 12 were based on a circuit model containing two RC branches. The absence of a second parallel resistance in the equivalent circuit model may have influenced the observed values of both the internal and parallel resistances.

These results indicate a relationship between the equivalent circuit parameters and the battery's state of charge. In particular, the response time shows a strong and consistent trend, suggesting it could be a useful indicator for estimating the state of charge as the battery depletes. However, these results were based on a single new battery and a single current profile. To ensure that the observed relationships hold across different batteries, current

profiles, and battery ages, a more comprehensive study is needed. This should include a larger sample size and greater variation in test conditions. Additionally, to improve the reliability of the equivalent circuit parameter estimates, the adaptation process should be optimised to yield more accurate and consistent values.

4.2.3 Battery weight

As zinc-air batteries discharge, zinc transforms into zinc oxide, resulting in an increase in battery weight. Additionally, most parasitic reactions in zinc-air batteries, such as self-discharge, corrosion and water loss, involve the ingress or egress of matter, which can be observed as a change in weight. By measuring the weight of zinc-air batteries, correlations between the battery weight and various properties such as lifetime, age and condition can be identified. Therefore, the weight of all size 13 zinc-air hearing aid battery cells from different manufacturers, ages, and conditions was measured before and after each discharge test.

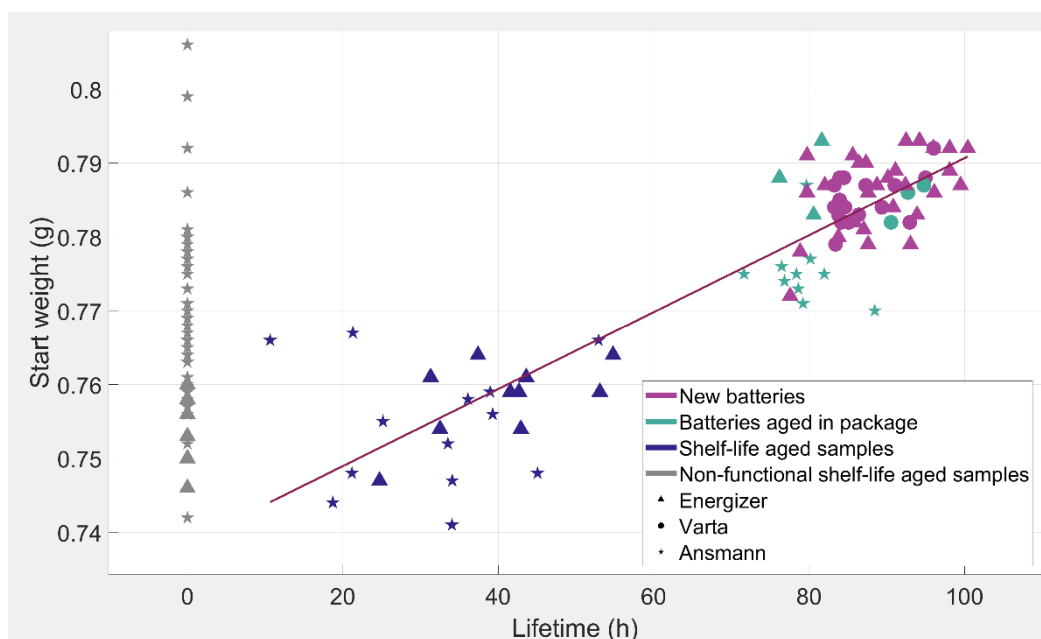


Figure 36: The lifetime and pre-discharge weight of every discharged battery

Figure 36 presents a scatter plot illustrating the pre-discharge weight and lifetime of each discharged battery. The aged batteries are lighter than the new ones, suggesting a loss of material over time as the batteries age. The pre-discharge weights and lifetimes of functional zinc-air batteries exhibit a roughly linear relationship, with batteries that start out heavier tending to have longer lifetimes and lighter batteries shorter lifetimes. This linear regression line is also depicted in Figure 36. The batteries appear to be

distributed along the weight axis according to their age and manufacturer. The heaviest batteries, which have the longest lifetimes, are the newest batteries, whose discharge curves are shown in Figure 24 and Figure 26. These batteries deviate the least from the regression line, likely due to the predictable behaviour of new batteries. In addition, a somewhat noticeable weight difference exists between manufacturers among the new batteries. Energizer batteries tend to be heavier than Varta batteries, which may explain the trend observed in discharge measurements, where Energizer batteries consistently demonstrated longer lifetimes than Varta batteries.

Below the new batteries are those aged in their original packaging, which exhibit slightly shorter lifetimes and lighter weights. Their discharge curves are shown in Figure 29 and Figure 30. Although their lifetimes somewhat overlap with those of the new batteries, they have clearly lost weight due to aging. This weight loss, rather than gain, suggests a probable loss of water, as both self-discharge and carbonate formation would result in weight gain. Despite deviating considerably from the regression line, their lighter weights still correlate with their shorter lifetimes.

Below the batteries aged in their original packaging are the functional shelf-life aged batteries, which have the shortest lifetimes and lightest weights. These batteries show the greatest deviation from the regression line, indicating that their behaviour is the most unpredictable. Additionally, there is no clear correlation between manufacturer and weight among the functional shelf-life aged batteries.

The weights of all non-functional shelf-life aged batteries were also measured. Among these, there is a clearer correlation between manufacturer and weight with Ansmann batteries tending to be heavier than Energizer batteries. This difference could be attributed to the manufacturer, but it may also be influenced by aging. All shelf-life aged Energizer batteries were only one year old, whereas the older batteries were exclusively Ansmann. If aging is the cause, it suggests that the batteries may initially lose weight due to water loss, followed by a weight increase likely caused by corrosion as the electrolyte becomes more concentrated as the battery dries out.

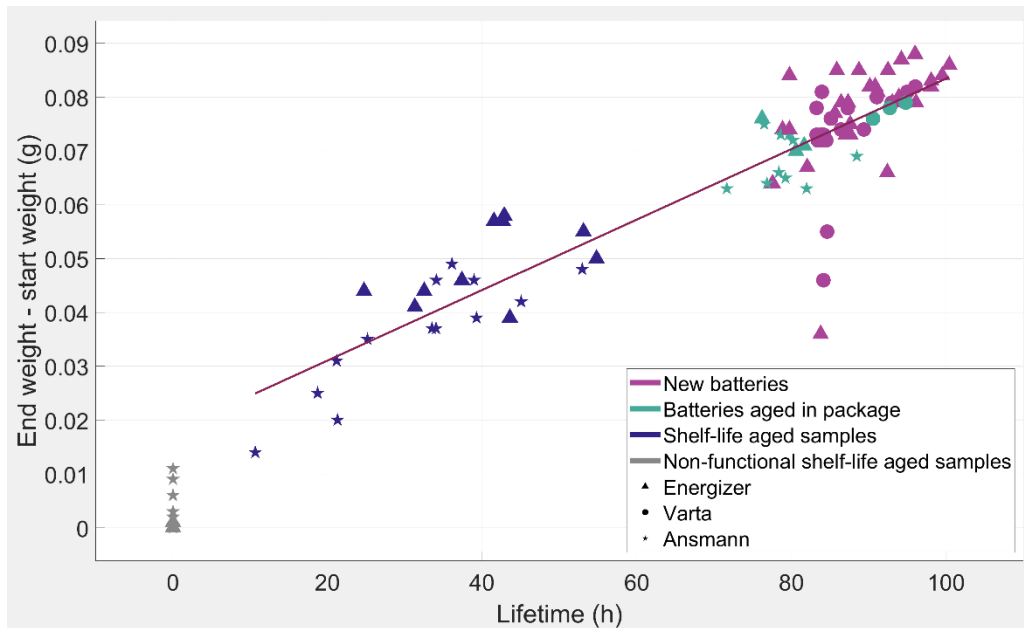


Figure 37: The lifetime and discharge induced weight change in every discharged battery

Figure 37 depicts a scatter plot illustrating the lifetimes and the difference between post-discharge and pre-discharge weight of all discharged batteries. The weight difference before and after discharge also exhibits a roughly linear relationship with the lifetime, as shown by the regression line in the figure. Batteries with longer lifetimes utilise a larger portion of the zinc inside, resulting in more zinc transforming into zinc oxide and leading to a greater change in weight. Additionally, non-functional batteries did not change in weight at all. The batteries deviate less from the regression line in Figure 37 compared to Figure 36, indicating that the weight change rather than the pre-discharge weight has a more dependent relationship with the battery's state of charge. However, it may be more beneficial to predict a battery's lifetime from its pre-discharge weight rather than from the weight change after discharge. Figure 37 shows no clear correlation between manufacturer and weight change, suggesting that the amount of material utilised during discharge is not influenced by the battery's manufacturer.

The weight measurements suggest that it is possible to predict the lifetime of zinc-air batteries to some extent based on their weight. This is particularly useful for aged batteries, whose lifetimes are linked to their weight. Weight can serve as an indicator for shelf-life aged batteries, helping to identify which ones are still functional and which ones are likely to have no charge left.

4.2.4 Investigation of battery aging through x-ray computed tomography

As a zinc-air battery discharges, the dense zinc within is converted into less dense zinc oxide, leading to an increase in the volume of the material inside the cell. This change in volume, along with the density difference between zinc and zinc oxide, can be visualised through CT imaging. To examine how aging affects the internal structure of the battery, shelf-life aged batteries were subjected to CT scans. For comparison, additional scans were performed on new zinc-air batteries that were fully discharged, partially discharged to 50%, and not discharged at all. Cross-sectional CT images of the intentionally discharged batteries can be seen in Figure 38.

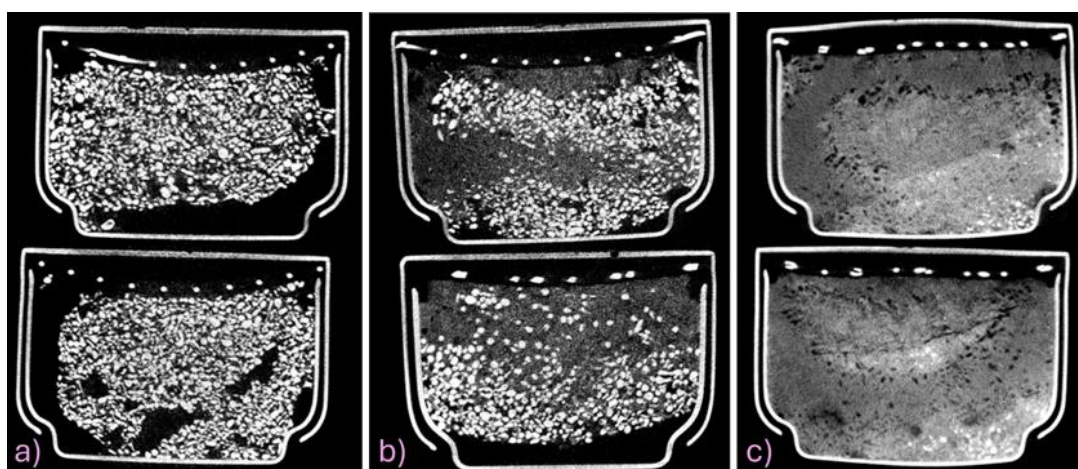


Figure 38: Cross-sectional CT images of batteries at a) 100%, b) 50%, and c) 0% state of charge. The upper and lower batteries in each panel are independent samples from the same manufacturer, treated identically in terms of discharge procedure.

Figure 38 shows CT images of zinc-air batteries that were deliberately discharged to different states of charge. In these images, the overall structure of the batteries is clearly visible. The internal material is enclosed by a metallic casing, which is divided into anode and cathode sections. At the top of each battery, there is a neat row of dots representing the cross-section of a metallic grid that serves as the current collector. The appearance of the internal material varies depending on the battery's charge level.

Figure 38 a) displays a battery that has not been discharged. There is a significant amount of empty space available to accommodate the expansion that occurs during discharge. The internal material appears to be entirely zinc, which is visible as bright, well-defined granules.

Figure 38 b) shows a battery that was discharged to 50% before imaging. About half of the internal material remains as zinc, while the other half has turned darker and cloudier, indicating the formation of zinc oxide. This zinc oxide is concentrated around the current collector, suggesting that oxidation begins near the collector and progresses inward. Although some empty space

remains, it is noticeably reduced compared to Figure 38 a), indicating an increase in material volume.

Figure 38 c) presents a fully discharged battery. Nearly all the internal material has transformed into zinc oxide, with only a few small clusters of bright zinc granules remaining at the bottom, farthest from the current collector. The internal space is almost completely filled, and the current collector is pressed flat against the casing. The battery casing appears to bend outwards at the top, showing how the material has expanded to occupy all available space.

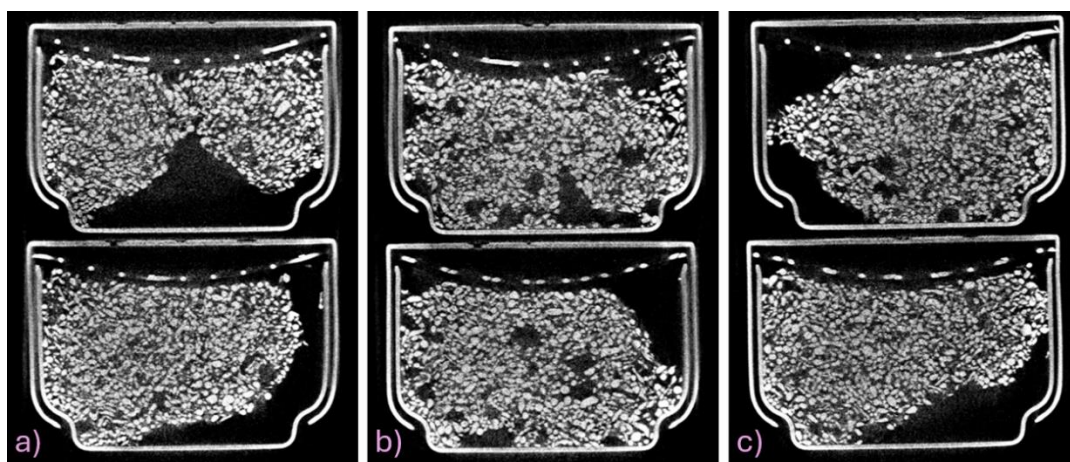


Figure 39: Cross-sectional CT images of shelf-life aged batteries whose equivalent samples remained functional. The batteries were manufactured and stored as follows: a) Ansmann, stored in an ESD bag since 2024, b) Energizer, stored in a CPP/OPP laminated bag since 2024, and c) Ansmann, stored in an ESD bag since 2023. The upper and lower batteries in each panel are independent samples from the same manufacturer, treated identically in terms of shelf-life aging procedure.

Figure 39 shows CT images of shelf-life aged batteries that have not been discharged. Shelf-life aged samples equivalent to these batteries were successfully activated, and their discharge curves are presented in Chapter 4.1.3. Visually, these aged batteries closely resemble the new, non-discharged battery shown in Figure 38 a), though subtle differences suggest the effects of aging.

All six batteries shown in Figure 39 display bright, well-defined granules that indicate the presence of zinc. The ample empty space within the casing suggests that there has been no significant increase in material volume. However, the overall appearance of the material is slightly darker and cloudier compared to the fresh battery. This cloudiness is distributed throughout the battery but is especially noticeable along the current collector. Since the current collector is located within the air electrode, an area that zinc cannot

access but that is saturated with electrolyte, the cloudiness likely reflects changes in the electrolyte rather than the zinc.

Two possible explanations appear plausible. One is the loss of water from the electrolyte, which would increase its concentration and potentially make it more visible in CT imaging. The other is a chemical reaction between the electrolyte and carbon dioxide from the air, which could lead to the formation of carbonate compounds.

Figure 39 a) shows Ansmann zinc-air batteries stored in ESD bags for one year. Figure 39 b) shows Energizer batteries stored in CPP/OPP laminated bags for the same duration. Figure 39 c) shows Ansmann batteries stored in ESD bags for two years. Despite the longer storage time for the batteries in Figure 39 c), the visual differences between the batteries are minimal. CT images of all batteries with equivalent shelf-life aged counterparts that were successfully activated also appear similar. This suggests that although signs of aging are detectable, determining the exact age or remaining lifetime of a battery based solely on CT imaging remains challenging. Cross-sectional CT images of the remaining imaged batteries are provided in Appendix D.

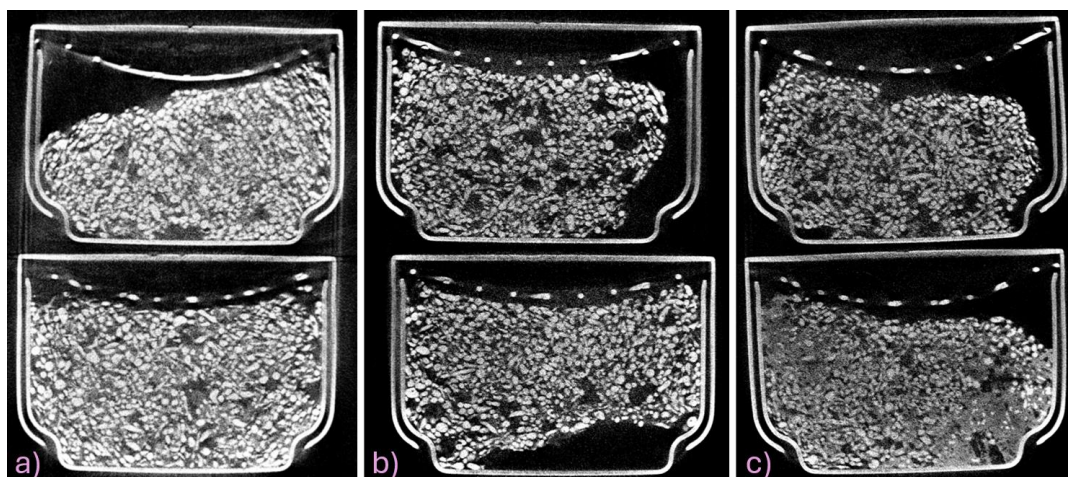


Figure 40: Cross-sectional CT images of shelf-life aged batteries whose equivalent samples were not functional. The batteries were manufactured and stored as follows: a) Ansmann, stored in a plastic zipper bag since 2023, b) Ansmann, stored in a plastic container since 2022 c) Ansmann, stored in its original package since 2022. The upper and lower batteries in each panel are independent samples from the same manufacturer, treated identically in terms of shelf-life aging procedure.

Figure 40 presents CT images of shelf-life aged batteries that have not been discharged. Equivalent samples of these batteries were rarely successfully activated. Compared to the functional batteries in Figure 39, the batteries in Figure 40 show greater variation in appearance. All six batteries still contain visible zinc granules, indicating that the lack of functionality is not due to complete zinc depletion. Additionally, each battery retains empty

space within the casing, also suggesting that the zinc has not significantly transformed into zinc oxide, which would otherwise increase the material volume. A common feature across all batteries in Figure 40 is the presence of cloudiness, similar to that observed in Figure 39, though its extent varies.

Figure 40 a) shows Ansmann batteries stored in plastic zipper bags since 2023. These are the newest among the batteries in Figure 40, which may explain why the zinc appears brightest. However, none of their counterparts in Chapter 4.1.3 were functional. This may be due to the pronounced cloudiness surrounding the zinc, possibly indicating changes in the electrolyte.

Figure 40 b) shows Ansmann batteries stored in plastic containers since 2022. These appear most similar to the functional batteries in Figure 39. Despite being of the oldest shelf-life aged batteries, a few equivalent samples were successfully activated. This aligns with the observation that these batteries show less apparent damage and only exhibit the same cloudy electrolyte near the current collector as seen in Figure 39.

Figure 40 c) shows Ansmann batteries stored in their original packaging, effectively exposed to open air, since 2022. These batteries, particularly the lower one, show the first signs of visible damage to the zinc. The battery contains distinct dark, cloudy regions consistent with the transformation of zinc, as seen in the depleted batteries in Figure 38. Interestingly, this transformation appears in scattered clusters rather than originating near the current collector, as is typical during discharge. This suggests that the zinc degradation may not be driven by electrochemical activity at the air electrode, but rather by prolonged exposure to the caustic electrolyte. All imaged batteries with equivalent shelf-life aged counterparts that were not functional exhibit varying degrees of the same types of damage observed in Figure 40. Cross-sectional CT images of the remaining batteries are included in Appendix D.

As zinc-air batteries age, structural damage within them becomes increasingly apparent. However, the extent of this damage appears to correlate with the level of exposure to ambient air. More airtight storage solutions, such as plastic containers, tend to result in less degradation compared to less airtight options like plastic zipper bags. The primary mechanism of aging seems to involve changes in the electrolyte, rather than direct corrosion of the zinc. Observable zinc degradation typically occurs only after prolonged exposure to both the electrolyte and ambient air.

4.3 Simulation of on/off battery control circuits

The functionality and leakage currents of battery control circuits were evaluated using transient simulations in LTspice. The circuits, originally described in Chapter 2.4.3, were modified to suit the requirements of a single-use clinical monitoring patch. The battery on/off control circuit must operate reliably across the full voltage range of three size 13 zinc-air hearing aid batteries connected in series. This range spans from approximately 3.75V when the

batteries are unused down to the UVLO threshold of 1.8V. Additionally, the control circuit needs to incorporate a momentary switch for user activation. The circuit should also respond to a 1.8V control signal from the MCU, which determines whether the device remains active. Circuit functionality was verified across the voltage range. Leakage current was assessed by measuring the current drawn from the power supply while the circuit was in its deactivated state with the assumption that the batteries were unused. To evaluate the impact of different transistors on leakage performance, the circuits were also simulated using a variety of commercially available transistor models.

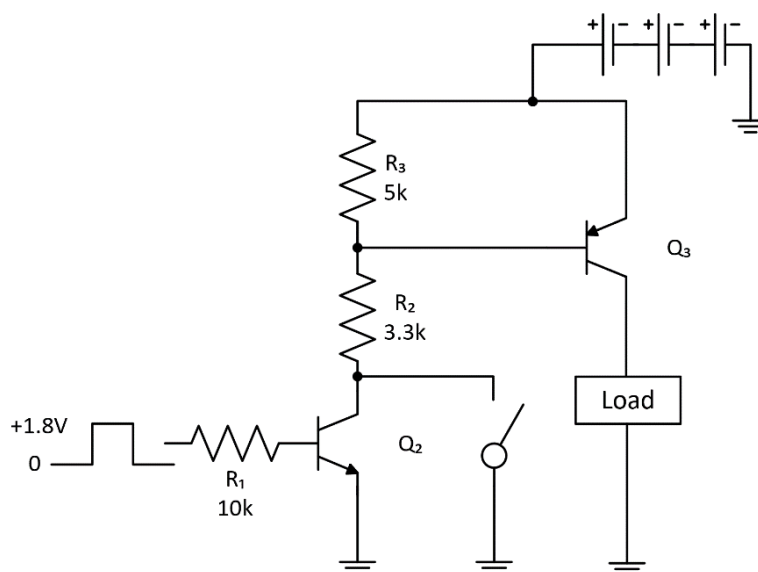


Figure 41: A BJT-based circuit that switches the high side of a load, adapted for use as an on/off battery control circuit

The circuit shown in Figure 17 B is a BJT-based circuit intended for high-side load switching. The circuit can be adapted to function as an on/off battery control circuit for the single-use clinical monitoring patch, as illustrated in Figure 41. This is achieved by incorporating a momentary switch, adjusting the power supply to match the voltage of three zinc-air batteries, and using a control signal from the MCU. The momentary switch allows the user to activate the pnp transistor Q_3 , which connects the batteries to the load and powers the device, including the MCU. Once powered, the MCU must output a 1.8V control signal to the base of Q_2 to maintain the device in its active state. Resistors R_2 and R_3 form a voltage divider that sets the base voltage of Q_3 . In the modified circuit shown in Figure 41, the value of R_3 was increased compared to the original circuit in Figure 17 B. This adjustment lowers the base voltage of Q_3 , ensuring that it can conduct properly under the reduced supply voltage.

When simulating the circuit in Figure 41 using LTspice, it was assumed that the momentary switch is initially held closed, and the MCU activates the 1.8V control signal immediately after the switch is released. The load in the simulation was configured to draw 3mA of current, which approximated the typical consumption of the single-use clinical monitoring patch during operation. The circuit’s functionality was verified, and leakage current was measured using SPICE models of various BJT transistors, all listed in Table 2. For each pair of transistors, the leakage current was recorded along with the specific transistor models and their unit price based on a quantity of more than 300,000 units from Mouser, a global electronic components distributor [39]. Most transistor combinations in Table 2 exhibited leakage currents around 40pA, except for the third combination, which showed a lower value of 18pA. These results appear unrealistically low when compared to the values in Table 3 and the general understanding that BJTs typically have higher leakage currents than MOSFETs. Since none of the transistor datasheets provide information on leakage current, it is possible that the LTspice models used do not accurately account for this parameter.

Table 2: BJTs used in high-side load switching circuit simulations

Transistor model	Position in circuit (Q_2/Q_3)	Price (€)	Leakage current
DTC124EE [40,41]	Q_2	0.039	37.516pA
BC857C [42]	Q_3	0.013	
BC846B [43]	Q_2	0.011	41.345pA
MMBTA92 [44,45]	Q_3	0.035	
BC817-16 [46]	Q_2	0.014	18.343pA
BC857B [47]	Q_3	0.011	
DTC143ZCA [48,49]	Q_2	0.022	37.516pA
DTA043TEB [50,51]	Q_3	0.022	
BC847B [52]	Q_2	0.011	41.312pA
MMBT2907A [53,54]	Q_3	0.015	

The circuit shown in Figure 41 can also be implemented using MOSFETs instead of BJTs. Since MOSFETs operate based on voltage rather than current, the resistor values are generally less critical. However, the voltage divider still sets the gate voltage of Q_3 . Increasing the value of R_3 lowers the gate voltage, allowing the use of transistors with higher threshold voltages. This not only broadens the selection of suitable transistors but may also help reduce leakage current, as higher threshold voltages often correlate with lower leakage.

The MOSFET-based version of the circuit was simulated under the same conditions as the BJT version. The transistor models, unit prices, and measured leakage currents are listed in Table 3. The value of R_3 was adjusted if

necessary for each transistor pair based on the threshold voltage of Q_3 , and these resistor values are also documented in Table 3.

The simulated leakage currents for the MOSFET circuits were at least three orders of magnitude higher than those of the BJT-based circuits, which appears implausible. According to the transistor datasheets, the gate-to-channel leakage current is approximately $\pm 100\text{nA}$, while the drain-to-source leakage is around $\pm 1\mu\text{A}$. These datasheet values suggest that the leakage currents reported in Table 3 are more realistic than those in Table 2. However, they are still subject to under- and overestimation due to limitations in the LTspice models. There was significant variation in leakage current between MOSFET pairs, which is unexpected given their datasheet specifications report very similar leakage currents. This suggests that differences in how accurately individual MOSFETs are modelled may be contributing to the observed variation.

Table 3: MOSFETs used in high-side load switching circuit simulations

Transistor model	Position in circuit (Q_2/Q_3)	Price (€)	Value of R_3 (Ω)	Leakage current
2N7002 [55]	Q_2	0.018	10k	41.018nA
PMV65XPE [56,57]	Q_3	0.085		
ZXM61No2F [58,59]	Q_2	0.136	20k	160.890nA
ZXMP6A13G [60,61]	Q_3	0.237		
Si8410DB [62,63]	Q_2	0.357	20k	694.695nA
Si6423DQ [64,65]	Q_3	0.749		

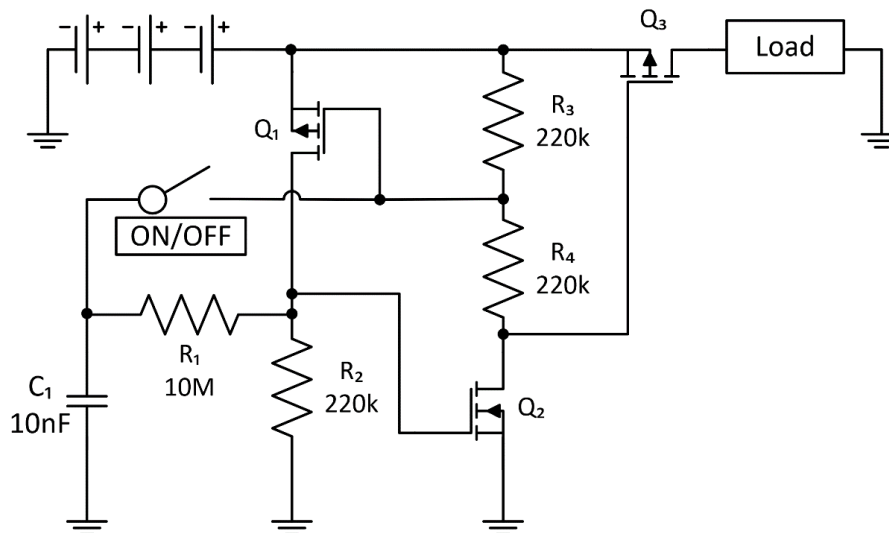


Figure 42: An on/off battery control circuit implemented with a MOSFET flip-flop and adapted for use in single-use clinical monitoring patch

The circuit presented in Figure 18 C is an on/off battery control circuit implemented using a complementary MOSFET flip-flop and a momentary

switch to toggle between its two stable states. To adapt this design for the single-use clinical monitoring patch, the circuit must be modified to operate within a lower voltage range of 1.8V to 3.75V, instead of the original 5V to 9V. For the transistors to function correctly at these lower voltages, either their threshold voltages must be reduced, or the gate voltages must be lowered. While most resistor values in the circuit were chosen based on optimal capacitor charge and discharge timing, resistors R_3 and R_4 also form a voltage divider that sets the gate voltage of Q_1 . The adapted version of the circuit is shown in Figure 42.

The circuit in Figure 42 was simulated across the full battery voltage range to verify correct toggling behaviour. Leakage current was simulated using various MOSFETs. Table 4 summarises the leakage values, transistor models, and transistor unit prices for each simulated circuit. The value of R_3 was adjusted in each simulation based on the threshold voltage of Q_1 , and these values are also documented in the table. The load was configured to draw 3mA, consistent with the expected current consumption of the monitoring patch.

Several of the MOSFETs used in the simulations were previously tested in the circuit from Figure 41, while others were selected from LTspice's built-in library. This was necessary because manufacturer-supplied models often caused the simulation to freeze. As a result, more models from LTspice were used, including one marked as obsolete in Table 4. Although there is some variation in leakage current among the tested transistors, with the first showing significantly higher leakage than the others, the average leakage current in the circuit from Figure 42 is somewhat lower than that of the circuit in Figure 41, even when using the same transistors. This suggests that the configuration in Figure 42 may be more effective at minimising leakage current, despite involving a greater number of transistors.

Table 4: MOSFETs used in simulations of the on/off battery control circuits implemented with a flip-flop

Transistor model	Position in circuit (Q_2/Q_3)	Price (€)	Value of R_3 (Ω)	Leakage current
Si4433DY [66]	Q_1	Obsolete	250k	718.729nA
2N7002 [55]	Q_2	0.018		
AO3423 [67]	Q_3	0.052		
PMV65XPE [56,57]	Q_1	0.085	250k	30.963nA
2N7002 [55]	Q_2	0.018		
ZXMP6A13G [60,61]	Q_3	0.237		
PMV65XPE [56,57]	Q_1	0.085	250k	31.352nA
2N7002 [55]	Q_2	0.018		
PMV65XPE [56,57]	Q_3	0.085		
RTQ035P02 [68]	Q_1	0.267	300k	27.105nA
BSP89 [69]	Q_2	0.163		

RTQ035P02 [68]	Q ₃	0.267		
----------------	----------------	-------	--	--

To make the circuit in Figure 42 fully suitable for the single-use clinical monitoring patch, it must also include a mechanism that allows the MCU's 1.8V control signal to decide whether the on/off battery control circuit remains active. While directly implementing this functionality can be challenging, an alternative approach is to give the MCU the ability to turn off the circuit when needed. This can be achieved by adding an NMOS transistor between the gate of Q₂ and ground, controlled by the 1.8V signal from the MCU. When the MCU wants to deactivate the device, it turns on the NMOS, pulling the gate of Q₂ to ground. This disables Q₂, which in turn disables Q₃ and sets the flip-flop into the off state.

Additionally, neither the circuit in Figure 41 nor the one in Figure 42 currently accounts for the PMU fuel gauge's measurement of the voltage of an individual battery, as shown in the system block diagram in Figure 3. To minimise leakage currents, this connection should also be controlled based on whether the device is on or off. One way to implement this is by placing an NMOS transistor between the individual battery voltage and the fuel gauge, with its gate connected to the output of the control circuit. This ensures that the fuel gauge is only connected when the battery is supplying power to the device. Alternatively, a PMOS transistor could be used for this purpose, controlled in the same way as the main PMOS switch that connects the battery to the rest of the device. However, care must be taken to ensure that the gate voltage is low enough to switch the PMOS correctly, given that it will be operating from the voltage of a single battery rather than three in series.

CMOS transmission gate circuits, such as the one shown in Figure 19, are available as integrated circuits with very low off-state leakage currents. A good example is the CD4066, a simple transmission gate IC that contains four independently controlled transmission gates, also known as channels. This component typically exhibits an off-state leakage current of only 10pA, and when purchased in bulk quantities of over 10,000 units, it costs just 0.291€ at Mouser [70]. This kind of transmission gate circuit would be relatively easy to implement as a battery control circuit. One of its channels could be used to control the connection between the battery and the rest of the device with the MCU's 1.8V control signal serving as the switch control. A momentary switch would still be needed alongside the MCU control signal to allow the user to initially activate the device. Additionally, another channel could be used to manage the connection between the fuel gauge and the individual battery voltage measurement. This channel could be controlled using the same signal as the main power switch.

Leakage current in the single-use clinical monitoring patch can be minimised using several different techniques. However, the methods are difficult to assess because the accuracy of the circuit simulations in LTspice are limited. For example, the simulated leakage currents of BJTs appear implausibly

low, while those of MOSFETs vary significantly between different models. This inconsistency arises from how transistors are modelled in LTspice, which often does not reflect real-world variations in device characteristics. Additionally, the simulations do not account for practical factors such as switch bounce or the delay between device activation and the MCU's response. In reality, the MCU may not react instantly after the user presses the momentary switch. If this delay is significant, a large enough capacitor may be needed to hold the circuit in the conducting state long enough to ensure proper startup. Ultimately, to obtain accurate leakage current values and validate circuit behaviour, the designs should be physically assembled and tested.

5 Conclusions and recommendations for future work

This thesis demonstrates that integrating zinc-air batteries into single-use clinical monitoring patches is feasible, provided their characteristics are well understood and properly managed. The results of this thesis show that these batteries can tolerate a wide range of current profiles, which aligns well with the fluctuating power demands of the patch. Despite the stable voltage output of zinc-air batteries, viable methods exist for monitoring their state of charge. In addition, zinc-air batteries exhibit promising performance over extended storage periods, making them suitable for devices with long shelf lives. Reliable techniques are also available for electrically isolating the batteries when the device is idle, helping to minimise leakage current and extend battery life.

The longest lifetimes for zinc-air batteries were observed when they were discharged under constant current conditions. However, in practical use, the single-use clinical monitoring patch draws current in intermittent pulses. Encouragingly, the batteries performed reliably under these fluctuating conditions, even during current peaks as high as 45mA. The primary effect observed was variation in battery lifetime depending on the specific current profile. To maximise battery performance, the device's current consumption could be optimised to follow a more favourable fluctuating profile. While some trends were identified linking current profile characteristics to battery longevity, further research is needed. This should include a larger sample size and a more controlled investigation into how specific parameters of fluctuating current affect battery longevity. Additionally, the combined effects of pulsed current consumption and battery aging over time warrant further exploration.

Zinc-air battery lifetime can be estimated using several different methods. The single-use clinical monitoring patch already includes a coulomb counter, which provides a foundation for tracking energy usage. However, to improve reliability, compensations must be developed to account for battery aging, and the precision of the coulomb counter itself should be evaluated. Response-time-based lifetime estimation also showed potential, but further investigation is needed. This includes testing with a larger sample size and applying a systematic optimisation method to determine whether a consistent relationship exists between response time and battery lifetime across all battery cells. Additionally, the influence of battery aging and varying current profiles on response time should be explored, and the feasibility of implementing the response time method in practice should be examined. Battery weight was also found to provide insight into discharge behaviour and could potentially be used at the time of installation to estimate remaining lifetime.

CT imaging proved useful in identifying the internal aging mechanisms of zinc-air batteries. Combined with discharge testing of shelf-life aged

batteries, the results suggest that degradation begins within months of the batteries' removal from their original packaging. However, earlier onset cannot be ruled out, as batteries aged less than one year were not tested. The extent of this degradation is strongly influenced by how well the storage method is sealed against ambient air. Storage solutions such as plastic containers and ESD bags, which offer effective sealing, resulted in the longest battery lifetimes. Despite these protective measures, the shelf life of zinc-air batteries appears to be limited to less than two years, as no batteries could be reliably activated after three years of storage. Further investigation is needed to better understand the aging process. Future studies should focus on shorter storage intervals and prioritise the most effective sealing methods identified so far. Additionally, the impact of storage container size, due to the amount of air present inside, should be explored. This would allow for a more detailed analysis of how storage duration and conditions impact battery performance over time.

The long storage times of the single-use clinical monitoring patches also necessitate a circuit solution that electrically isolates the batteries from the device when it is not in use, in order to prevent depletion due to leakage currents. In a single-use device, cost-effectiveness is also a critical consideration. Several transistor-based switching circuits, using both BJTs and MOSFETs, were shown to function effectively. This included configurations with added features, such as a user-activated on/off switch and a controlled connection between the fuel gauge and the voltage of an individual battery being monitored. These circuits maintained minimal leakage current, even with low-cost components. Ultimately, the decision of which circuit to use and if additional features should be included depends on whether the benefits justify the cost of extra components. Fortunately, all proposed solutions remain relatively inexpensive, as the circuits performed well with affordable transistors. However, to properly evaluate the suitability of these circuits, real-world testing is essential. Simulations do not properly capture important factors such as leakage current, switch bounce, or delays in MCU response. Physical prototyping and measurement are therefore necessary to validate the performance and reliability of these circuit solutions.

With their tolerance for varying current profiles, extended shelf life, and reliable performance, zinc-air batteries are a highly promising power source for single-use clinical monitoring patches. They have demonstrated the ability to withstand the operational demands of the device, and with further research, their integration could be optimised even further. Future studies focusing on battery aging, current profile optimisation, and real-world circuit validation will be essential to fully realise their potential. As the demand for single-use medical technologies continues to grow, zinc-air batteries stand out as a compact, cost-effective, and reliable energy source well-suited for this application.

References

- [1] D. Q. Brown, "Disposable vs Reusable Electrocardiography Leads in Development of and Cross-contamination by Resistant Bacteria," *Critical Care Nurse*, vol. 31, no. 3, pp. 62-68, June 2011, doi: 10.4037/ccn2011874.
- [2] Y. Zhong, B. Liu, Z. Zhao, Y. Shen, X. Liu and C. Zhong, "Influencing Factors of Performance Degradation of Zinc–Air Batteries Exposed to Air," *Energies*, vol. 14, no. 9, p. 2607, May 2021, doi: 10.3390/en14092607.
- [3] M. Amaral, F. do Vale, J. Silva, F. Caramelo and G. Veiga, "In Vitro Zinc-Air Battery Evaluation for Use in Intraoral Medical Devices," *Journal of Medical Devices*, vol. 8, no. 1, pp. 014509, March 2014, doi: 10.1115/1.4026450.
- [4] E. Sanal, P. Dost and C. Sourkounis, "Electrotechnical investigation of Zinc-Air Cells for determination of Cell-Parameters for a Battery Management System," in *4th International Conference on Renewable Energy Research and Applications*, Palermo, Italy, 2015, pp. 1157-1161, doi: 10.1109/ICRERA.2015.7418591.
- [5] T. Arlt, D. Schröder, U. Krewer and I. Manke, "In operando monitoring of the state of charge and species distribution in zinc air batteries using X-ray tomography and model-based simulations," *Physical Chemistry Chemical Physics*, vol. 16, no. 40, pp. 22273-22280, September 2014, doi: 10.1039/c4cp02878c.
- [6] J. J. Nance, H. L. Hess and T. B. Atwater, "An Ultra Low Current Low Cost Zinc-Air Battery Discharge Monitor Utilizing a Microcontroller Based Countdown Algorithm," in *Twenty-First Annual IEEE Applied Power Electronics Conference and Exposition, 2006, APEC '06*, Dallas, USA, 2006, pp. 4, doi: 10.1109/APEC.2006.1620602.
- [7] R. M. Dondelinger, "Batteries: from alkaline to zinc-air," *Biomedical Instrumentation & Technology*, vol. 38, no. 2, pp. 100-110, March 2004, doi: 10.2345/0899-8205.
- [8] Y. Li and H. Dai, "Recent advances in zinc–air batteries," *Chemical Society Reviews*, vol. 43, no. 15, pp. 5257-5275, June 2014, doi: 10.1039/C4CS00015C.
- [9] Abbott Diabetes Care, "FreeStyle Libre 3 Continuous Glucose Monitoring System User's Manual," [Online]. Available: https://freestyleserver.com/Payloads/IFU/2022/q2/ART46090-003_rev-A.pdf. [Accessed 25 March 2025].
- [10] A. Nguyen and J. R. White, "FreeStyle Libre 3," *Clinical Diabetes*, vol. 41, no. 1, pp. 127-128, Oct 2022, doi: 10.2337/cd22-0102.
- [11] Healthline, "Product Review: Abbott FreeStyle Libre Flash Glucose Monitor," August 2018 [Online]. Available:

- <https://www.healthline.com/diabetesmine/abbott-freestyle-libre-review#bottom-line>. [Accessed 20 March 2025].
- [12] M. Yenikomshian et al., “Cardiac arrhythmia detection outcomes among patients monitored with the Zio patch system: a systematic literature review,” *Current Medical Research and Opinion*, vol. 35, no. 10, pp. 1659-1670, May 2019, doi: 10.1080/03007995.2019.1610370.
- [13] iRhythm Technologies, Inc., “Zio XT Clinical Reference Manual,” [Online]. Available: <https://www.irhythmtech.com/content/dam/irhythm/united-states/ifus/february-updates/NLB0020.08%20-%20ZIO%20XT%20CLINICAL%20REFERENCE%20MANUAL.pdf>. [Accessed 25 March 2025].
- [14] R. A. Powers, “Batteries for Low Power Electronics,” *Proceedings of the IEEE*, vol. 83, no. 4, pp. 687-693, April 1995, doi: 10.1109/5.371974.
- [15] J. Hack, D. Patel, J. J. Bailey, F. Iacoviello, P. R. Shearing and D. J. L. Brett, “In situ x-ray computed tomography of zinc–air primary cells during discharge: correlating discharge rate to anode morphology,” *Journal of Physics: Materials*, vol. 5, no. 1, p. 014001, December 2021, doi: 10.1088/2515-7639/ac3f9a.
- [16] X. Chen, Z. Zhou, H. E. Karahan, Q. Shao, L. Wei and Y. Chen, “Recent Advances in Materials and Design of Electrochemically Rechargeable Zinc–Air Batteries,” *Small*, vol. 14, no. 44, p. 1801929, August 2018, doi: 10.1002/smll.201801929.
- [17] J. Stamm, A. Varzi, A. Latz and B. Horstamm, “Modeling nucleation and growth of zinc oxide during discharge of primary zinc-air batteries,” *Journal of Power Sources*, vol. 360, pp. 136-149, August 2017, doi: 10.1016/j.jpowsour.2017.05.073.
- [18] J.-S. Lee et al., “Metal-Air Batteries with High Energy Density: Li-Air versus Zn-Air,” *Advanced Energy Materials*, vol. 1, no. 1, pp. 34-50, December 2010, doi: 10.1002/aenm.201000010.
- [19] A. Abbasi, S. Hosseini, A. Somwangthanaroj, R. Cheacharoen, S. Olaru and S. Kheawhom, “Discharge profile of a zinc-air flow battery at various electrolyte flow rates and discharge currents,” *Scientific Data*, vol. 7, no. 196, June 2020, doi: 10.1038/s41597-020-0539-y.
- [20] V. Pop, “State-of-the-art of battery state-of-charge determination,” *Measurement Science and Technology*, vol. 16, no. 12, October 2005, doi: 10.1088/0957-0233/16/12/R01.
- [21] H. E. Lin, C. H. Ho and C. Y. Lee, “Discharge performance of zinc coating prepared by pulse electroplating with different frequencies for application in zinc-air battery,” *Surface and Coatings Technology*, vol. 319, pp. 378-385, June 2017, doi: 10.1016/j.surfcoat.2017.04.020.

- [22] L. M. Feeney, C. Rohner, P. Gunningberg, A. Lindgren and L. Andersson, "How do the dynamics of battery discharge affect sensor lifetime?," in *11th Annual Conference on Wireless On-demand Network Systems and Services*, Obergurgl, Austria, 2014, pp. 49-56, doi: 10.1109/WONS.2014.6814721.
- [23] L. A. Tinker, "Advances in Air Manager Technology for Zinc-Air Batteries," in *Sixteenth Annual Battery Conference on Applications and Advances*, Long Beach, USA, 2001, pp. 319-322, doi: 10.1109/BCAA.2001.905147.
- [24] A. Kube, J. Meyer, D. Kopljar, N. Wagner and K. A. Friedrich, "A Segmented Cell Measuring Technique for Current Distribution Measurements in Batteries, Exemplified by the Operando Investigation of a Zn-Air Battery," *Journal of the Electrochemical Society*, vol. 168, no. 12, p. 120530, December 2021, doi: 10.1149/1945-7111/ac4059.
- [25] X. Hu, F. Feng, K. Liu, L. Zhang, J. Xie and B. Liu, "State estimation for advanced battery management: Key challenges and future trends," *Renewable and Sustainable Energy Reviews*, vol. 114, October 2019, doi: 10.1016/j.rser.2019.109334.
- [26] W.-Y. Chang, "The State of Charge Estimating Methods for Battery: A Review," *ISRN Applied Mathematics*, vol. 2013, no. 1, July 2013, doi: 10.1155/2013/953792.
- [27] J. D. Pineda-Rodriguez, S. Olaru, C. Vlad, P. Rodriguez-Ayerbe, W. Lao-Atiman and S. Kheawhom, "Model-based dynamical voltage prediction of Zinc-Air cell for piecewise discharge currents," *2023 9th International Conference on Control, Decision and Information Technologies (CoDIT)*, Rome, Italy, 2023, pp. 2538-2543, doi: 10.1109/CoDIT58514.2023.10284056.
- [28] J. K. R. Franke-Lang and J. Kowal, "An equivalent circuit zinc-air battery model by impedance spectroscopy," in *IV Metal-advanced Batteries International Congress*, Pamplona, Spain, November 2019, doi: 10.13140/RG.2.2.16222.05440.
- [29] K. Lahiri, A. Raghunathan, S. Dey and D. Panigrahi, "Battery-driven system design: a new frontier in low power design," in *Proceedings of ASP-DAC/VLSI Design 2002. 7th Asia and South Pacific Design Automation Conference and 15th International Conference on VLSI Design*, Bangalore, India, 2002, pp. 261-267, doi: 10.1109/ASPDAC.2002.994932.
- [30] G. Marin-Garcia, G. Vazquez-Guzman, J. M. Sosa, A. R. Lopez, P. R. Martinez-Rodriguez and D. Langarica, "Battery Types and Electrical Models: A Review," in *2020 IEEE International Autumn Meeting on Power, Electronics and Computing (ROPEC)*, Ixtapa, Mexico, 2020, pp. 1-6, doi: 10.1109/ROPEC50909.2020.9258711.

- [31] M. Pedram and Q. Wu, "Design Considerations for Battery-Powered Electronics," in *Proceedings 1999 Design Automation Conference*, New Orleans, LA, USA, 1999, pp. 861-866, doi: 10.1109/DAC.1999.782166.
- [32] A. Jossen, "Fundamentals of battery dynamics," *Journal of Power Sources*, vol. 154, no. 2, pp. 530-538, March 2006, doi: 10.1016/j.jpowsour.2005.10.041.
- [33] S. S. Rajput and S. S. Jamuar, "Low voltage analog circuit design techniques," *IEEE Circuits and Systems Magazine*, vol. 2, no. 1, pp. 24-42, 2002, doi: 10.1109/MCAS.2002.999703.
- [34] T. Jain, "Analysis of Li-Ion Battery Characteristics in a Wearable Patient Monitoring Device Using Equivalent Circuit Model," Master's Thesis, Aalto University, Espoo, Finland, February 2021.
- [35] L. Hu and X. Xu, "Current Pulse-Based Measurement Technique for Zinc-Air Battery Parameters," *Energies*, vol. 16, no. 18, p. 6448, September 2023, doi: 10.3390/en16186448.
- [36] P. Horowitz and W. Hill, *The Art of Electronics*, 3rd Edition, Cambridge, U.K.: Cambridge University Press, 2015, pp. 71-222.
- [37] A. S. Sedra, K. C. Smith, T. C. Carusone and V. Gaudet, *Microelectronic Circuits*, 8th Edition, New York, NY, USA: Oxford University Press, 2020, pp. 244-364.
- [38] Energizer, "Product Datasheet," [Online]. Available: <https://data.energizer.com/pdfs/13.pdf>. [Accessed 26 March 2025].
- [39] Mouser Electronics, "Electronic Components Distributor - Mouser Electronics Europe", [Online]. Available: <https://eu.mouser.com/>. [Accessed 23 May 2025].
- [40] Octopart, "ROHM DTC124EETL", [Online]. Available: <https://octopart.com/dtc124eetl-rohm-355737>. [Accessed 17 May 2025].
- [41] ROHM, "DTC124EE", [Online]. Available: <https://www.rohm.com/products/transistors/digital-transistors/standard/dtc124ee-product#productDetail>. [Accessed 17 May 2025].
- [42] Octopart, "Diode BC857C", [Online]. Available: <https://octopart.com/bc857c-diotec-22658687>. [Accessed 17 May 2025].
- [43] Octopart, "Nexperia BC846B,215", [Online]. Available: <https://octopart.com/bc846b%2C215-nexperia-78739092>. [Accessed 17 May 2025].
- [44] Octopart, "Diodes Inc. MMBTA92Q-7-F", [Online]. Available: https://octopart.com/detail/all_breaks?sid=e1a42c2e1b833e63¤cy=EUR. [Accessed 17 May 2025].
- [45] Diodes, "MMBTA92", [Online]. Available: <https://www.diodes.com/part/view/MMBTA92/>. [Accessed 17 May 2025].

- [46] Octopart, "Diotec BC817-16", [Online]. Available: <https://octopart.com/bc817-16-diotec-30744424>. [Accessed 17 May 2025].
- [47] Octopart, "Diotec BC857B", [Online]. Available: <https://octopart.com/bc857b-diotec-30744653>. [Accessed 17 May 2025].
- [48] Octopart, "ROHM DTC143ZCAHZGT116", [Online]. Available: <https://octopart.com/dtc143zcahzt116-rohm-82941477>. [Accessed 17 May 2025].
- [49] ROHM, "DTC143ZCA", [Online]. Available: <https://www.rohm.com/products/transistors/digital-transistors/standard/dtc143zca-product#productDetail>. [Accessed 17 May 2025].
- [50] Octopart, "ROHM DTA043TEBTL", [Online]. Available: <https://octopart.com/dta043tebtl-rohm-30943670>. [Accessed 17 May 2025].
- [51] ROHM, "DTA043TEB", [Online]. Available: <https://www.rohm.com/products/transistors/digital-transistors/standard/dta043teb-product#productDetail>. [Accessed 17 May 2025].
- [52] Octopart, "Nexperia BC847B,235", [Online]. Available: <https://octopart.com/bc847b%2C235-nexperia-78739106>. [Accessed 17 May 2025].
- [53] Octopart, "Diodes Inc. MMBT2907A-7-F", [Online]. Available: <https://octopart.com/mmbt2907a-7-f-diodes+inc.-55389596>. [Accessed 17 May 2025].
- [54] Diodes, "MMBT2907A", [Online]. Available: <https://www.diodes.com/part/view/MMBT2907A/>. [Accessed 17 May 2025].
- [55] Octopart, "Diotec 2N7002", [Online]. Available: <https://octopart.com/2n7002-diotec-109206764>. [Accessed 17 May 2025].
- [56] Octopart, "Nexperia PMV65XPEAR", [Online]. Available: <https://octopart.com/pmv65xpear-nexperia-78741647>. [Accessed 17 May 2025].
- [57] Nexperia, "PMV65XPE", [Online]. Available: <https://www.nexperia.com/product/PMV65XPE>. [Accessed 17 May 2025].
- [58] Octopart, "Diodes Inc. ZXM61No2FTA", [Online]. Available: <https://octopart.com/zxm61no2fta-diodes+inc.-660002>. [Accessed 17 May 2025].
- [59] Diodes, "ZXM61No2F", [Online]. Available: <https://www.diodes.com/part/view/ZXM61No2F/>. [Accessed 17 May 2025].

- [60] Octopart, "Diodes Inc. ZXMP6A13GTA", [Online]. Available: <https://octopart.com/zxmp6a13gta-diodes+inc.-660153>. [Accessed 17 May 2025].
- [61] Diodes, "ZXMP6A13G", [Online]. Available: <https://www.diodes.com/part/view/ZXMP6A13G>. [Accessed 17 May 2025].
- [62] Octopart, "Vishay SI8410DB-T2-E1", [Online]. Available: <https://octopart.com/si8410db-t2-e1-vishay-57062128>. [Accessed 17 May 2025].
- [63] Vishay, "SI8410DB Product Information", [Online]. Available: <https://www.vishay.com/en/product/62961/>. [Accessed 17 May 2025].
- [64] Octopart, "Vishay SI6423DQ-T1-GE3", [Online]. Available: <https://octopart.com/si6423dq-t1-ge3-vishay-42303812>. [Accessed 17 May 2025].
- [65] Vishay, "SI6423DQ Product Information", [Online]. Available: <https://www.vishay.com/en/product/72257/>. [Accessed 17 May 2025].
- [66] Octopart, "SI4433DY-T1-E3", [Online]. Available: <https://octopart.com/si4433dy-t1-e3-vishay-40889197>. [Accessed 17 May 2025].
- [67] Octopart, "Alpha & Omega Semiconductor AO3423", [Online]. Available: <https://octopart.com/ao3423-alpha+%26+omega+semiconductor-12432285>. [Accessed 17 May 2025].
- [68] Octopart, "ROHM RTQ035P02HZGTR", [Online]. Available: <https://octopart.com/rtq035p02hzgtr-rohm-104803834>. [Accessed 17 May 2025].
- [69] Octopart, "Nexperia BSP89,115", [Online]. Available: <https://octopart.com/bsp89%2C115-nexperia-78739354>. [Accessed 17 May 2025].
- [70] Octopart, "Texas Instruments CD4066BE", [Online]. Available: <https://octopart.com/cd4066be-texas+instruments-3103>. [Accessed 17 May 2025].

A. LabVIEW program for producing fluctuating discharge currents

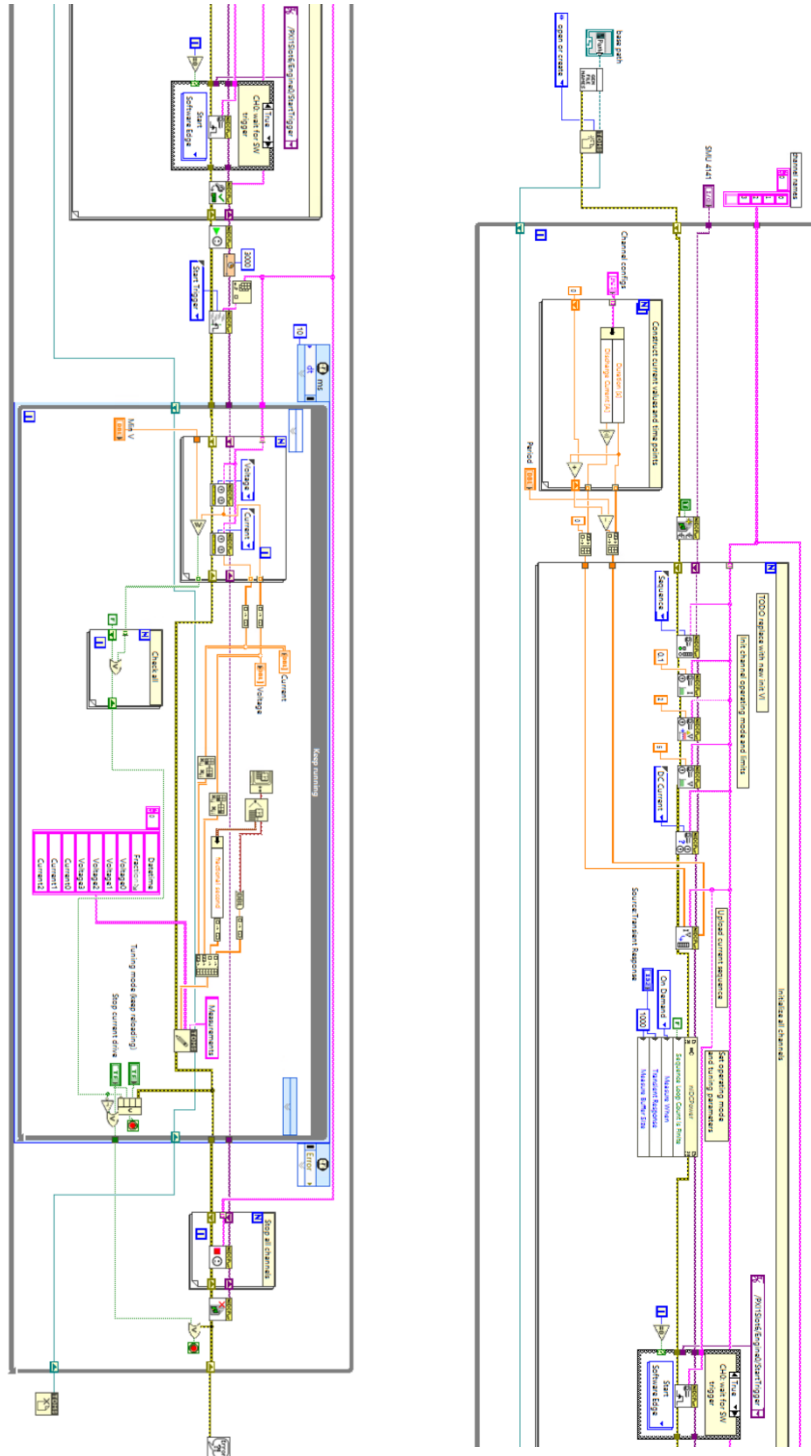


Figure A1: The provided LabVIEW program for producing fluctuating discharge currents

B. Storage methods for shelf-life battery aging



Figure B1: Heat sealed CPP/OPP laminated bags



Figure B2: Heat sealed ESD bags



Figure B3: Original packaging. The tabs covering the holes in the casing were removed.

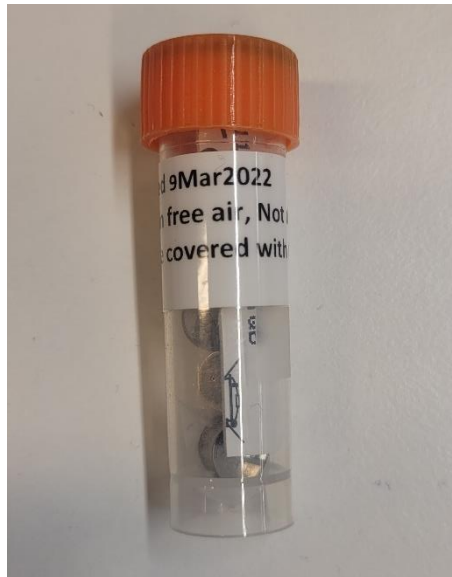


Figure B4: Plastic container



Figure B5: Plastic zipper bag

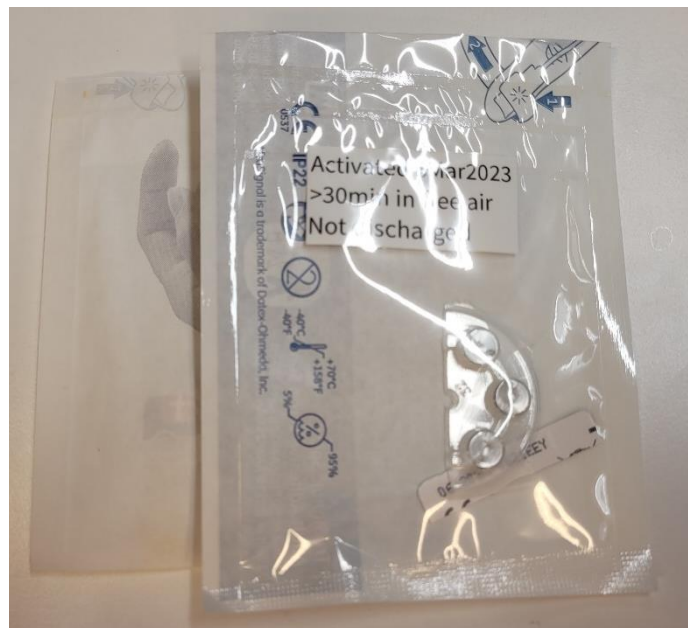


Figure B6: Paper/plastic bags, a standard packaging method for medical accessory products

C. Equivalent circuit modelling results

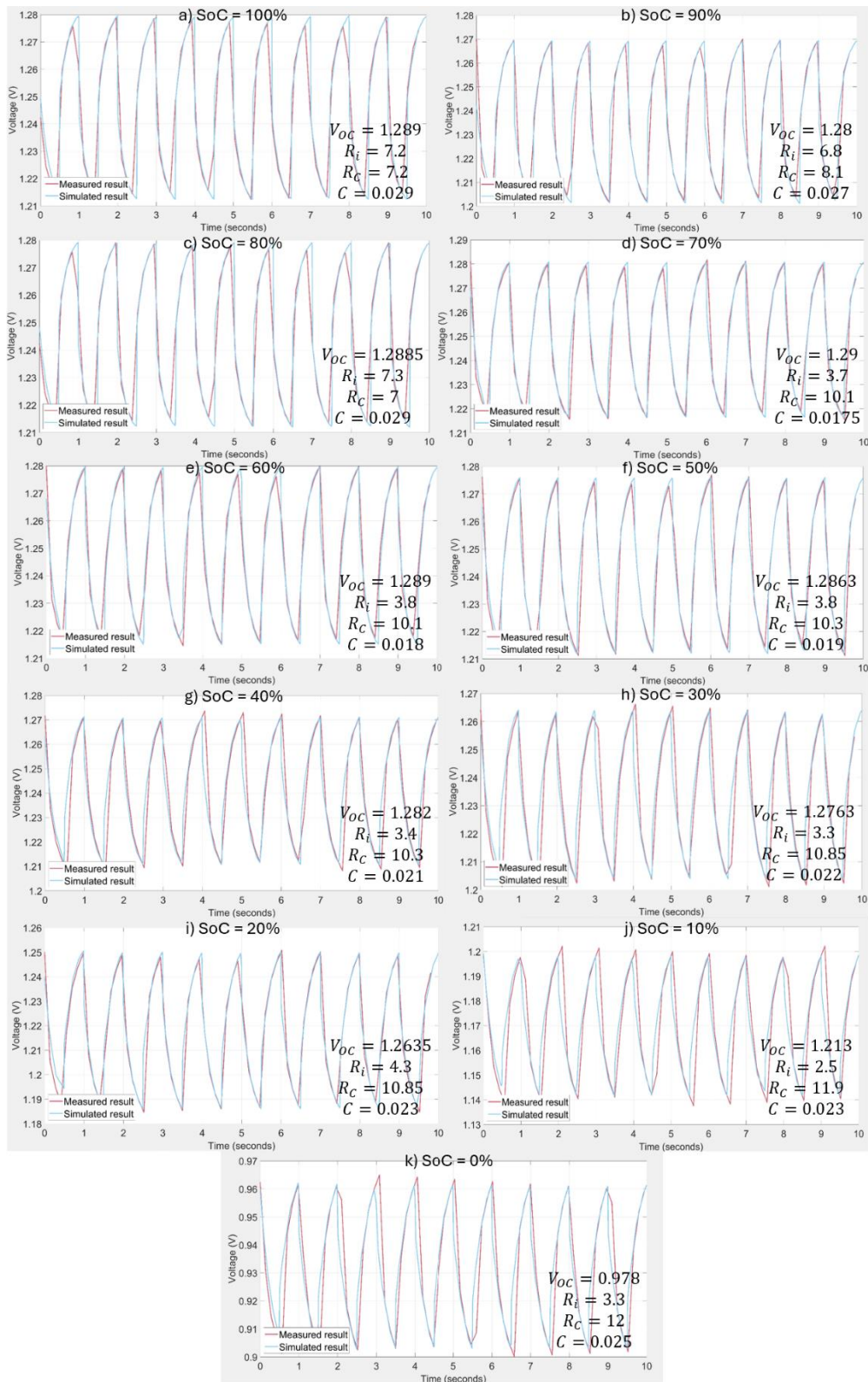


Figure C1: Equivalent circuit component adaption over battery lifetime

D. Cross-sectional CT images of zinc-air batteries

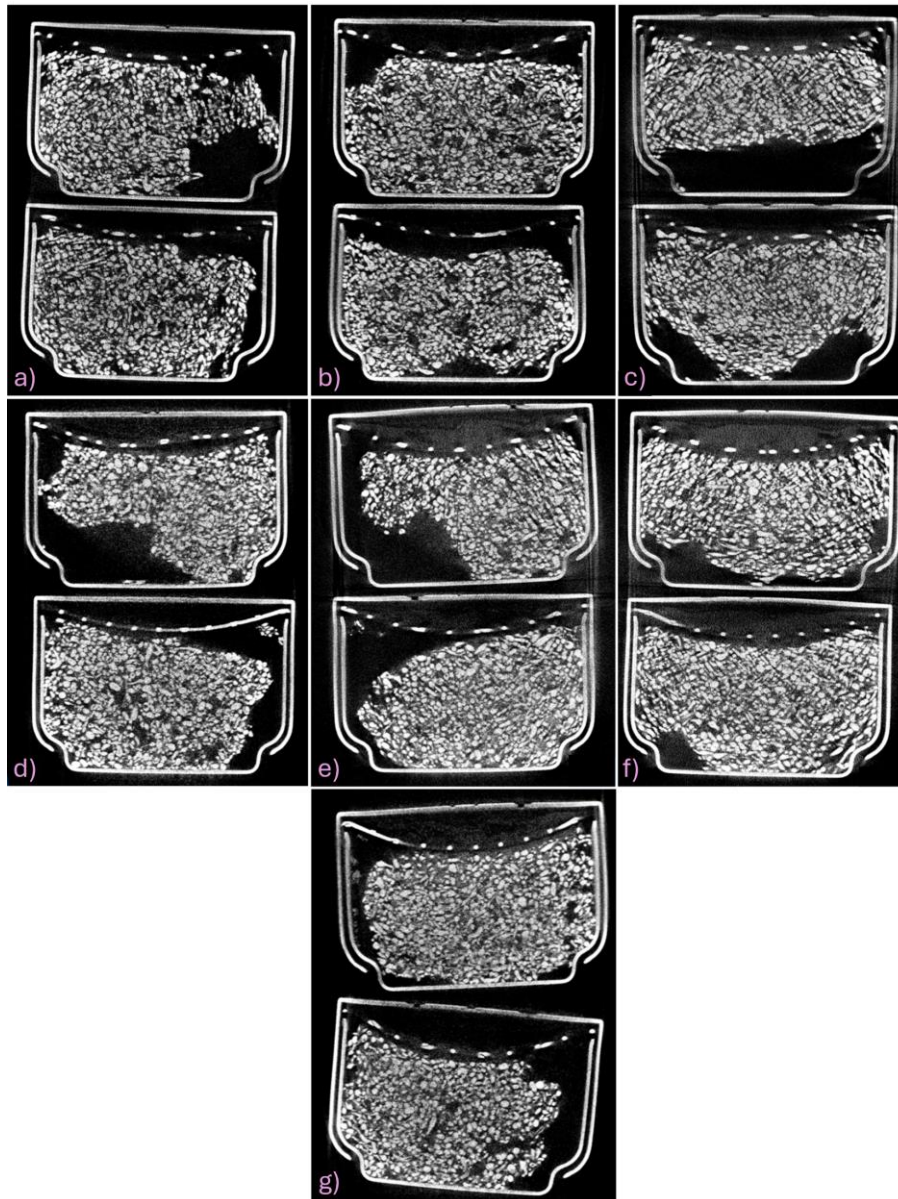


Figure D1: Cross-sectional CT images of shelf-life aged batteries. The batteries were manufactured and stored as follows: a) Ansmann, stored in a plastic container since 2024, b) Ansmann, stored in a CPP/OPP bag since 2024, c) Energizer, stored in an ESD bag since 2024, d) Ansmann, the upper stored in a plastic zipper bag since 2023 and the lower stored in an acrylic container since 2022, e) Ansmann, stored in its original package since 2024, f) Energizer, stored in its original package since 2024, g) Ansmann, stored in a paper/plastic bag since 2023. The upper and lower batteries in each panel are independent samples from the same manufacturer, treated identically in terms of shelf-life aging procedure with the exception of d).